Accepted Manuscript

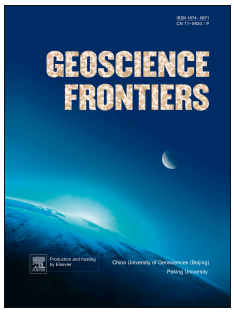

Interaction between protokimberlite melts and mantle lithosphere: evidence from mantle xenoliths from the Dalnyaya kimberlite pipe, Yakutia (Russia)

I.V. Ashchepkov, T. Ntaflos, Z.V. Spetsius, R.F. Salikhov, H. Downes

PII: S1674-9871(16)30051-2

DOI: 10.1016/j.gsf.2016.05.008

Reference: GSF 458

To appear in: *Geoscience Frontiers*

Received Date: 26 January 2016

Revised Date: 27 April 2016

Accepted Date: 1 May 2016

Please cite this article as: Ashchepkov, I.V., Ntaflos, T., Spetsius, Z.V., Salikhov, R.F., Downes, H., Interaction between protokimberlite melts and mantle lithosphere: evidence from mantle xenoliths from the Dalnyaya kimberlite pipe, Yakutia (Russia), *Geoscience Frontiers* (2016), doi: 10.1016/j.gsf.2016.05.008.

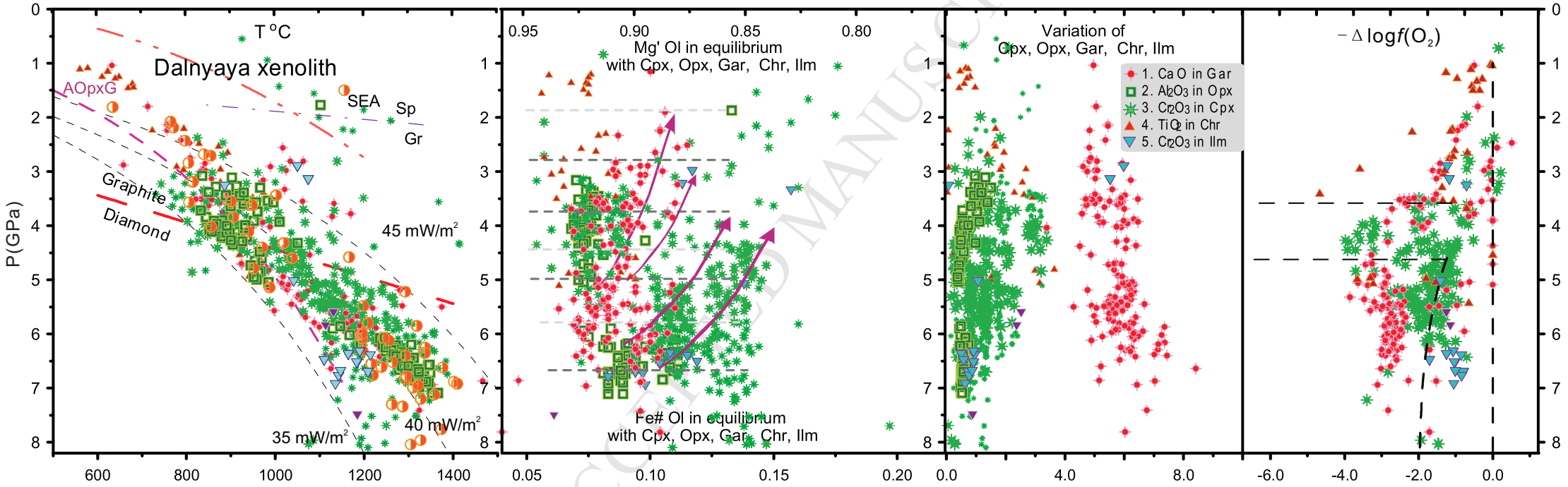

Interaction between protokimberlite melts and mantle lithosphere: evidence from mantle xenoliths from the Dalnyaya kimberlite pipe, Yakutia (Russia)

I.V. Ashchepkov[a,*], T. Ntaflos[b], Z.V. Spetsius[c], R.F. Salikhov[c], H. Downes[d]

[a] *Institute of Geology and Mineralogy, SD RAS, Koptyug avenue 3, 63090, Novosibirsk, Russia*

[b] *Vienna University, A-1090 Vienna, Austria*

[c] *Alrosa Stock Company, Mirny,Lenina 6, Russia*

[d] *Department of Earth and Planetary Sciences, Birkbeck University of London, London, UK*

*Corresponding author e-mail address: Igor.Ashchepkov@igm.nsc.ru; garnet@igm.nsc.ru; igora57@mail.ru

phone (fax): 007-950-5918327

fax institute: 007 -383-2332792

Abstract

The Dalnyaya kimberlite pipe (Yakutia, Russia) contains mantle peridotite xenoliths (mostly lherzolites and harzburgites) that show both sheared porphyroclastic (deformed) and coarse granular textures, together with ilmenite and clinopyroxene megacrysts. Deformed peridotites contain high-temperature Fe-rich clinopyroxenes, sometimes associated with picroilmenites, which are products of interaction of the lithospheric mantle with protokimberlite related melts. The orthopyroxene-derived geotherm for the lithospheric mantle beneath Dalnyaya is stepped similar to that beneath the Udachnaya pipe. Coarse granular xenoliths fall on a geotherm of 35 mWm^{-2} whereas deformed varieties yield a 45 mWm^{-2} geotherm in the 2–7.5 GPa pressure interval. The chemistry of the constituent minerals including garnet, olivine and clinopyroxene shows trends of increasing $Fe^{\#}$ (= Fe/(Fe+Mg) with decreasing pressure. This may suggest that the interaction with fractionating protokimberlite melts occurred at different levels. Two major mantle lithologies are distinguished by the trace element patterns of their constituent minerals, determined by LA-ICP-MS. Orthopyroxenes, some clinopyroxenes and rare garnets are depleted in Ba, Sr, HFSE and MREE and represent relic lithospheric mantle. Re-fertilized garnet and clinopyroxene are more enriched. The distribution of trace elements between garnet and clinopyroxene shows that the garnets dissolved primary orthopyroxene and clinopyroxene. Later high temperature clinopyroxenes related to the protokimberlite melts partially dissolved these garnets. Olivines show decreases in Ni and increases in Al, Ca and Ti from Mg-rich varieties to the more Fe-rich, deformed and refertilized ones. Minerals showing higher $Fe^{\#}$ (0.11–0.15) are found within intergrowths of low-Cr ilmenite-clinopyroxene-garnet related to the crystallization of protokimberlite melts in feeder channels. In *P-f*(O_2) diagrams, garnets and Cr-rich clinopyroxenes indicate reduced conditions at the base of the lithosphere at -5 log units below a FMQ buffer. However, Cr-poor clinopyroxenes, together with ilmenite and some Fe-Ca-rich garnets, demonstrate a more oxidized trend in the lower part of lithosphere at -2 to 0 log units relative to FMQ. Clinopyroxenes from xenoliths in most cases show conditions transitional between those determined for garnets and megacrystalline Cr-poor suite. The relatively low diamond grade of Dalnyaya kimberlites is explained by a high degree of interaction with the oxidized protokimberlite melts, which is greater at the base of the lithosphere.

Key words: mantle xenoliths; trace element; melt interaction; kimberlite; pyrope; Cr-diopside

1. Introduction

Mantle xenoliths brought to the surface by kimberlite eruptions show a wide variety of compositions and textures. One of the most important problems in understanding the formation such xenoliths is determining primary features (i.e. those present in the mantle before kimberlite activity began) and secondary ones superimposed on the mantle peridotites prior to (or during) entrainment in the host kimberlite. Here we present a study of mantle material from the Dalnyaya kimberlite pipe in Siberia giving evidence for interaction of the mantle with fractionating protokimberlite melts.

The Dalnyaya pipe, discovered in 1955, is one the largest kimberlite pipes (390 × 270 m) in the Daldyn field. Like most large pipes in the central part of the Yakutian kimberlite province (YKP) (Fig. 1A), Dalnyaya has a Late Devonian age (Agashev et al., 2004; Zaitsev and Smelov, 2010; Smelov et al., 2014). It is located in the southeastern part of the Daldyn field (Fig. 1B). The pipe is composed of two major group I (Mitchell, 1995) kimberlite varieties, both containing large amounts of debris mainly macrocrystic olivine (Cas et al., 2008). Autolithic kimberlite breccia (AKB) dominates the northern and eastern parts, whereas massive magmatic porphyritic kimberlite (PK) forms bodies in the northern and southeastern parts. It has a relatively low diamond grade compared to Aykhal, Udachnaya, Yubileinaya and other pipes which are being mined, and its greater distance from the mining centers did not allow industrial exploration to start earlier. Nevertheless, the overall diamond capacity is 10.2 million carats with total price of about 600,000 dollars, has allowing industrial work to start (Interfax, 2015). In 2011 a new 30 m-deep prospecting quarry was excavated within the central part of the pipe which is composed of PK, in contact with AKB. Both kimberlite varieties contain large amounts of mantle xenoliths, dominantly peridotites with relatively fresh pyroxenes and olivines.

In this paper, we have investigated mineral compositions from xenoliths and concentrates of both PK and ABK facies using electron probe micro analyzes (EPMA) and LA-ICP-MS, and have reconstructed the mantle section beneath the pipe as has been previously done for the Sytykanskaya pipe (Ashchepkov et al., 2015). The occurrence of abundant Cr-poor, Fe-rich clinopyroxenes and the unusually large amounts of ilmenite intergrowths and ilmenite-bearing xenoliths, including garnet wehrlites and Cr-bearing peridotites, suggest a high degree of interaction of protokimberlites with mantle peridotites, which probably influenced the diamond grade.

2. Samples

All ~300 xenoliths studied were collected from the newly excavated quarry in August-September, 2012. They are relatively fresh and contain fresh pyroxenes and even olivines. Commonly they are 3-10 cm in size. We did not separate samples from AKB and PK in this study. The latter contains more abundant and fresher xenoliths, but megacrysts and their intergrowth in AKB are more abundant. Large garnet-ilmenite-clinopyroxene intergrowths described in previous publications (Rodionov et al., 1988, 1991) were not found, because the quarry mainly exposes PK facies.

3. Analytical methods

Preliminary analyses were made of 40 xenoliths in thin-section using the Camebax Micro electron microprobe in IGM SB RAS. In addition, more than 75 xenoliths were analyzed in thin sections at the University of Vienna. For more than 30 high precision microprobe analyses were done for two crystals per sample. We also analyzed minerals from concentrates of PK (370) and ABK (420) facies separately, whereas minerals of an additional ~50 mantle xenoliths were analyzed in grain-mounts. Previous studies of the Dalnyaya pipe were devoted to the comparison of indicator minerals between the two kimberlite phases (Rodionov et al., 1984), and to the intergrowths of pyrope garnet, clinopyroxene and ilmenite megacrysts, and the ilmenite-bearing peridotites and pyroxenites (Rodionov et al., 1988, 1991). Analyses from a previous study of ilmenite-chromite-diopside intergrowths (Ashchepkov et al., 2014) were also included in the data base as well as analyses of ilmenite-bearing garnet pyroxenites from Rodionov et al. (1988, 1991) and Genshaft et al. (1987).

The procedure of the Electron Probe Microanalysis (EPMA) used for the analyses of concentrates and xenoliths in mounts in IGM SB RAS is described by Lavrent'ev et al. (1987). Routine conditions and precision of the analyses of Camebax Micro microprobe were also published (Sobolev et al., 1973, 2009a; Lavrent'ev and Usova, 1994; Ashchepkov et al., 2010a, 2012, 2013a,b, 2014, 2015). The detailed work on xenoliths (75) in thin sections was done at the University of Vienna using a Cameca100-SX microprobe. All analyses were done using mineral standards with wavelength-dispersive spectrometers; acceleration voltage and beam current were 15 kV and 20 nA, respectively, and standard correction procedures were applied. Trace elements in olivines from xenoliths were also performed with the Cameca 100SX. For the high precision

analyses of olivine, the acceleration voltage of 20 kV, a slightly defocused beam current of 60 nA were applied. In order to increase the precision and reduce the effect of noisy background on very low elemental concentrations, a 120 second counting time on peak position and on both low and high background positions, were used. As standard for the major elements (Si, Fe, Mg, Ca) natural olivine was used and for Ni, Cr, Al, Mn, metal alloys was used. Precision varies from 7 to 25 ppm for trace elements in olivine like Ni, Cr, Al, Mn and Ca.

Mineral concentrates were analyzed by laser ablation inductively coupled LA-ICP-MS at the Analytic Centre of IGM SB RAS (Ashchepkov et al., 2008). An additional 52 LA-ICP-MS analyses were obtained with the same equipment for minerals in thin sections of the xenoliths studied by EPMA in Vienna University (Supplementary File 1, Tables 1, 2). Analyses of trace elements of xenoliths in mounts and thin sections were obtained by LA- ICP-MS methods using a Finnegan Element I mass spectrometer and laser ablation system Nd YAG: UV New Wave 133 nm in Analytic Center of IGM SD RAS. The details were described in previous publications (Ashchepkov et al., 2012, 2013a, b, c, 2014a, b, 2015; Afanasiev et al., 2014).

4. Petrographic description of the xenoliths

The set of >300 xenoliths covers the petrographic variations in the lithospheric mantle beneath the Dalnyaya pipe (Fig. 2). Most of them are rather small (1 to 3 cm) and it is difficult to judge their structure using such small amounts of material.

The xenoliths belong to both the green Cr-bearing suite and black low-Cr suite described in previous publications (Rodionov et al., 1993). Most of them are relatively fertile or depleted garnet lherzolites (Fig. 2I) (25 vol. %) and harzburgites (Fig. 2P, U) (15 vol. %) (Fig. 3). Garnets in fertile xenoliths are only partly altered but in coarse grained harzburgites they are intensely kelyphitized. Many xenoliths (> 45 vol. %) contain bright emerald-green Cr-diopsides which form veins and micro-veins (Fig. 2E, Q, W), sometimes together with rather large bright red rounded garnets. Xenoliths which are unusually enriched in garnets and clinopyroxenes (Fig. 2G, J),(i.e. tending towards garnet websterites) constitute 5–7 vol. % of the studied collection. Garnet dunites (Fig. 2X) are very scarce (1–2 vol. %). Spinel harzburgites (Fig. 2p) comprise >12–10 vol. %. Giant-grained pyroxenites with parallel lamellae of orthopyroxene and rare garnets (Fig. 2D) occur very rarely (<2 vol. %). Typical eclogites were not discovered in this

collection but clinopyroxene-garnet-ilmenite intergrowths were described previously (Rodionov et al., 1988, 1991).

Garnet peridotites frequently show porphyroclastic textures (Fig. 2H, K, L, R) with two generations of olivine and intergranular Cr-diopsides. Sometimes olivine aggregates are grouped into clusters which may originally represent large olivine grains are now recrystallized (Fig. 2H, K, R). The coarse-grained peridotites are rare and mainly are represented by depleted harzburgites with or without garnet. Some xenoliths are composed of rounded polycrystalline fragments (Fig. 2T) cut by dark aggregates including pyroxenes, ilmenites (Fig. 2M) and sulfides cemented by more Fe-rich olivines. Ilmenite grains commonly together with Fe-rich pyroxenes are located in intergranular spaces together with mica and sulfides which are often replaced by djerfisherite. Ilmenite peridotites from Dalnyaya are texturally unequilibrated (Fig. 2M, Q) and differ from those found in Sytykanskaya (Ashchepkov et al., 2015) and Udachnaya pipes (Pokhilenko et al., 1976). Abundant mica veinlets were found in one Dalnyaya peridotite, and in rare cases mica is accompanied by richterite amphiboles (Supplementary File 4).

In the Dalnyaya megacryst associations, ilmenite is more abundant than garnet and chromite. Elliptical ilmenite nodules up to 8 cm in diameter often containing clinopyroxene and olivine inclusions and intergrowths (Fig. 2A, B, C) occur in the ABK. Garnet-ilmenite-clinopyroxene associations including giant-grained varieties are more common in ABK facies than in PK.

5. Chemistry of minerals

Compositions of pyrope garnets from concentrates mostly fall in the lower part of the lherzolite field (Sobolev et al., 1973) with concentrations of Cr_2O_3 reaching 13 wt. %. Some plot in the harzburgite and even dunite fields (Fig. 3), whereas garnets from xenoliths generally fall in the lherzolite field. Wehrlitic garnet megacrysts or those from the low-Ca xenolith suite contain up to 2.5 wt. % Cr_2O_3 or even belong to the Cr-rich group. The Cr-rich garnets from xenoliths have higher TiO_2 concentrations. The PK contain higher amount of both sub-calcic and pyroxenitic garnets compared to xenoliths and ABK garnet populations.

All Cr-bearing clinopyroxenes from the kimberlite heavy fractions have low Al contents. A few Al-rich varieties (up to 6 wt. % Al_2O_3) are found among the Fe-rich samples (up to 4.5 wt. % FeO) in ilmenite-bearing and porphyroclastic peridotites (Fig. 4). Na_2O contents, together with Cr_2O_3 and MgO, decrease with increasing FeO, whereas TiO_2 is nearly constant.

Orthopyroxenes which contain 4–5 wt. % FeO show increases of Al_2O_3 and CaO (Supplementary File 2, Fig. 3), decreases of Cr_2O_3 and NiO, and high scatter in TiO_2. As the content of FeO reaches 7 wt. %, Al_2O_3 and Cr_2O_3 decrease and CaO and TiO_2 become constant.

Ilmenites from AKB and PK show similar trends but the latter shows higher scatter in NiO, Al_2O_3 and Cr_2O_3. Two sub-trends dividing at 51 wt. % TiO_2 are seen in ilmenites from the AKB (Fig. 5). The first show stable Cr_2O_3 contents at ~ 0.9 wt. % whereas Mg- and Ti-rich varieties show variations in Cr_2O_3 ~0.5–1.2 wt. % and dispersion of other components.

Ilmenites in the peridotite xenoliths, as well as those from the intergrowths with clinopyroxenes, belong mainly to the Mg-rich type (up to 16 wt. % MgO). Significant differences in the TiO_2–Al_2O_3 trends suggest that ilmenites from AKB and PK were formed in different stages. However, ilmenites from Dalnyaya do not show the division into three groups which is typical for the pipes from the Zarnitsa cluster (Amshinsky and Pokhilenko, 1983).

Chromites are rarely found in the xenoliths; they occur mostly in the rims of garnets and in the Garnet-free chromite-bearing lherzolites. They show three major intervals in Cr_2O_3 and only a few plot within the diamond window. In chromite from the xenoliths, TiO_2 enrichment increases with Cr_2O_3 (i.e. with increasing pressure) (Fig. 6), but Cr-content is much higher (35–55 wt. % Cr_2O_3) in chromites from the concentrates.

Phlogopites are relatively scarce in xenoliths from Dalnyaya compared with the Alakit field pipes like Sytykanskaya (Ashchepkov et al., 2015). Most phlogopites occupy positions in the variation diagrams just on the boundary between scattered grains and typical micro-veined phlogopite-bearing associations and may relate to interaction with intergranular melts as was determined for xenoliths from the Sytykanskaya pipe (Ashchepkov et al., 2015) (Fig. 7).

The richterite amphiboles from Dalnyaya xenoliths are K-Na type (see Supplementary File 4) and differ from those found in peridotite xenoliths from Alakit kimberlites which are mostly K-rich (Ashchepkov et al., 2015).

Four large clusters and six small groups of olivines can be distinguished from their variations of trace components vs. $Fe^{\#}$. The first cluster (I) is a low-Fe group ($Fe^{\#}$ = 0.05–0.6) which comprises relic peridotites corresponding to Archean dunites. Cluster II with $Fe^{\#}$=0.07–0.9 is composed of fertile peridotites, whereas several samples (Cluster III) with $Fe^{\#}$=0.09–0.10 may be related to refertilized peridotites. We consider that the most Fe-rich group (Cluster IV) with $Fe^{\#}$=0.11–0.13 is related to interaction with protokimberlite melts. In general, the magmatic components Ca, Al, Mn show increases with $Fe^{\#}$, but Ti and Cr demonstrate more complex

trends in separate intervals (Fig. 8). General decrease of Ni is common and is explained by interaction with the essentially carbonatitic and kimberlite melts (Bussweiler et al., 2014).

6. Thermobarometry

6.1 Comparison of pressure-temperature (PT) estimates for mantle lithosphere beneath the Dalnyaya pipe

The pyroxene geotherm with the inflection at 6 GPa (Boyd, 1973) constructed for Lesotho was reproduced for sub-continental lithospheric mantle (SCLM) beneath Udachnaya in Daldyn field (Boyd et al., 1997) and appeared again for the SCLM beneath Dalnyaya pipe.

P–T estimates based on orthopyroxene thermobarometry yield the most reliable geotherm according to our comparisons (Ashchepkov et al., 2010, 2011, 2012, 2013a, b, c, 2014). Opx barometry was widely used in mantle reconstructions (Finnerty and Boyd, 1984). We used for the construction of the simple and reliable geotherm the combination (McGregor, 1974; Brey and Kohler, 1990) (Fig. 9A). Opx-based and Gar-Opx methods (Nickel and Green, 1985; Nickel, 1989; Brey and Kohler, 1990) (Fig. 9A, B, C) respectively, with the Opx or Opx-Cpx (Brey and Kohler, 1990) thermometers produce nearly coinciding PT plots (Wu and Zhao, 2011).

The mantle lithosphere beneath the Dalnyaya pipe is layered and shows two major pressure intervals with a gap from 5 to 6 GPa, while beneath the Udachnaya pipe this interval is represented by coarse Gar-harzburgites and eclogites (Ashchepkov et al., 2012, 2014) (see Supplementary File 2, Fig. 5). In the SCLM beneath Udachnaya there are 6 definite layers in the lithospheric mantle and the number of rock-types is higher (Ashchepkov et al., 2010, 2013b; 2014; Ionov et al., 2010). At least four groups from the lower and middle part of the Dalnyaya mantle section are close or nearly the same as those determined from the Udachnaya SCLM (see Supplementary File 2, Fig. 5B). The low-T group from 5 to 6 GPa is represented on *P–T* diagram for Dalnyaya by several points. The middle group corresponding to a pyroxenite layer (Pokhilenko et al., 1999) is cooler. The shallowest groups which are common in Udachnaya SCLM are not represented, mainly because the samples with large Cpx and Gar grains were analyzed while the shallow depleted harzburgites were omitted.

Comparison of different combinations of thermometers and barometers shows that PT estimates using Gar-Opx barometry (Nickel and Green, 1985; Brey and Kohler, 1990) (Fig. 9A,B,C) practically reproduces the Opx geotherm. The Cr–Cpx -based geotherm (Nimis and

Taylor, 2000) (Fig. 9D) reproduces the same groups as the Opx-based PT points but show displacement to higher pressures for the Fe-Cr-bearing compositions. The Cpx method based on jadeite-diopside exchange for the peridotitic and pyroxenitic associations (Ashchepkov et al., 2011) (Fig. 9E) shows that the high pressure branch composed of the sheared and porphyroclastic peridotites consists of two separate groups which differ in temperature. In general, it produces the much higher temperature geotherm probably related to the protokimberlite stage. This universal Cpx-based thermobarometry which could be applied to the low-Cr basic and Cr-rich ultrabasic and eclogitic systems (Ashchepkov et al., 2011) (Fig. 9 E) also traces all the Opx-points but the proportion of the high temperature associations is much greater. The reason is not only in the difference in thermometry but also that the lower-Cr associations were not used for thermometry by Cr-Cpx methods.

The garnet geotherm (Ashchepkov et al., 2015) (Fig.9E) traces practically all the groups of the orthopyroxene geotherm but continues into the higher pressure part, showing that the interval from 6 to 5 GPa is rather depleted in orthopyroxenes as well as the low pressure part.

The chromite-based geotherm (Supplementary File 2, Fig.5) corresponds mainly to the middle and low pressure intervals. Ilmenite-based PT estimates from the xenoliths (Supplementary File 2, Fig.5) reflect the conditions of high pressure interactions in the lower part of the mantle section and of mantle metasomatism in the middle part accompanied by formation of phlogopite and amphiboles.

6.2 P–T–X–f(O_2) reconstructions of mantle sections

The *P–T–f*(O_2) estimates based on the monomineral thermobarometry (Ashchepkov et al., 2010, 2012, 2013a, b, c, 2014a, b, 2015) enable us to make PTXfO_2 diagrams for all xenoliths samples together (Fig. 10A) and separately for the concentrates (Fig. 10B, C) as was previously done for the Sytykanskaya pipe (Ashchepkov et al., 2015). In general, the geotherm for minerals from xenoliths is very similar to that for the mantle beneath the Udachnaya pipe (Ashchepkov et al., 2013). The *P*–$Fe^{\#}$ plot shows several garnet trends demonstrating increasing $Fe^{\#}$ with decreasing pressure (see the arrows) which are common in mantle columns worldwide (Fig. 10A, B, C) (Ashchepkov et al., 2010, 2012, 2013a, b, c). Clinopyroxene and even olivine (pressure determined from the associated Cpx) repeats these trends; possibly this is the result of some rapidly differentiated melts in different pressures in the mantle column formed in several stages. Clinopyroxene and ilmenites in *P*–$Fe^{\#}$ plot often relate to the most Fe-rich branches

corresponding to the Ilm-Cpx intergrowths near the lithosphere base. The *P–T–X–f*(O_2) diagram for the xenoliths shows that many associations are not equilibrated, the Cpx are often much more Fe-rich compared to the garnets and olivines and this is not a temperature- dependent Fe-Mg distribution (Krogh, 1988; Kohler and Brey, 1990). The garnet *P*–CaO trends are divided into three lines with different CaO contents. The higher values are typical for garnets near the lithosphere asthenosphere boundary (LAB) and the highest values are in garnets of the pyroxenite-wehrlite associations. They are related to fertilization processes produced by carbonatitic protokimberlite melts (Howarth et al., 2014; Pokhilenko et al., 2015).

The *P–T–X* diagrams based on minerals from the concentrates are divided (Fig. 10B,C) into two parts at 4.0 GPa. The *P*–$Fe^{\#}$ trends show a rapid increase of FeO with decreasing pressures corresponding to the evolution of ilmenite trend produced by the protokimberlites. The AKB concentrates demonstrate some enrichment of garnets in CaO and FeO from 3.5 to 4.5 GPa compared with those from PK. This suggests the presence of pyroxenites in the middle part of the mantle column. The ilmenite trend in *P*–$Fe^{\#}$ diagrams is divided into two intervals at $Fe^{\#}$=0.12, probably related to two stages of protokimberlite evolution.

In the *P–f*(O_2) diagram (Fig. 10), the garnets and several clinopyroxenes near 5 GPa show a trend which is common for the SCLM worldwide (McCammon et al., 2001; McCammon and Kopylova, 2004), showing increasingly reduced conditions with depth. The ilmenite trend traces the diamond stability as in the Sytykanskaya pipe (Ashchepkov et al., 2015) which suggests relatively close *f*(O_2) conditions for megacrystic associations derived from protokimberlites and megacrystic clinopyroxenes. Some increase in *f*(O_2) occurs in the lower part of the SCLM and several garnet points are located within the oxidized field, coinciding with the oxygen fugacity conditions for the ilmenites and clinopyroxenes, which in general resemble the oxygen fugacity of protokimberlite melts (Höfer et al., 2009).

This highly oxidized level is marked also by several Gar, Cpx and Ilm points near 3 GPa. Oxidized associations correspond to the essentially carbonatitic compositions of the kimberlitic parental melts, according to the lines of CO_3^{2-} concentrations (Stagno et al., 2013).

The *P–T–X–f*(O_2) diagrams for the xenoliths (Fig. 10A) also show the presence of two major pressure intervals in SCLM divided at 3.5 GPa. The lower part shows a high degree of heating which is commonly associated with sheared mantle and is often related to interaction with protokimberlite melts (Agashev et al., 2013; Ashchepkov et al., 2013b) as in the SCLM beneath the Udachnaya pipe. However, in the Dalnyaya pipe they are represented by porphyroclastic and micro-veined peridotites. Their *P–T* points on diagram (Figs. 9, 10) are

marked by orthopyroxene, orthopyroxene-garnet and clinopyroxene thermobarometry and form convection branch below 6 GPa (Boyd et al., 1997). Clinopyroxene *P–T* estimates yield hotter geotherms compared with those produced by other minerals. Temperatures based on the two pyroxene methods (Wells, 1977; Taylor et al., 1979; Brey and Kohler, 1990) are higher than those that are orthopyroxene-based (Brey and Kohler, 1990). So the orthopyroxene-based geotherms are essentially cooler than Cpx-only estimates (Nimis and Taylor, 2000). The common Gar-Opx barometry (Nickel and Green, 1985; Brey and Kohler, 1990) in combination with the two pyroxene temperature gives similar or slightly hotter conditions than the orthopyroxene-based method.

Garnets in the *P*–$Fe^{\#}$ diagram reveal linear trends in the lower part of diagram and also in the upper part which definitely differ from those determined for concentrates from kimberlites. The upper interval is divided at 3.0–2.5 GPa showing irregular heating and increasing of Fe# for garnets and pyroxenes. The lowest pressure interval 1.0–2.0 GPa is again highly heated and represented by the Fe-rich associations.

The *P*–$f(O_2)$ diagram for garnets from xenoliths shows a linear decreasing $f(O_2)$ trend from -3.5 to -1.5 ΔFMQ in the pressure interval from 7.5 to 2GPa, which is narrower than the range shown by the minerals from concentrates (Fig. 10A). Ilmenites from the xenoliths show a rather wide range in Cr_2O_3 up to 6 wt. % at near 3.5 GPa. Clinopyroxenes mostly correspond to more oxidizing conditions than garnets. The presence of several Ilm *P*–$Fe^{\#}$ trends as well as for Gar and Cpx suggest that the lower and middle parts of the peridotite mantle column were subject to several stages of melt percolation.

7. Trace elements

7.1. Trace elements in peridotitic minerals

Trace element concentrations in garnet, clinopyroxene and ilmenite grains from the concentrates (Supplementary File 1, Tables 1, 2) and xenoliths are generally very similar (Figs. 11, 12). Garnets mainly show HREE-enriched round patterns, although those from concentrates have higher HREE compared with those from xenoliths, which show a dominant harzburgitic pattern with a slight depression from Yb to Dy or sometimes a humped pyroxenitic pattern with a peak at Sm (Fig. 11C). All garnets have strong depressions in Sr, Ba, Zr–Hf and Ta–Nb. Garnet of dunitic type has deep trough from Sm to Yb. Garnets from the mineral concentrates from kimberlites mostly have similar round patterns. Some of them show slightly lower HREE

content and only one belongs to the depleted dunitic type with the inflected REE pattern close to S-type, but it does not show a deep high field strength element (HFSE) trough (Supplementary File 2, Fig. 13).

Among the clinopyroxenes, the dominant type shows an asymmetric bell-like pattern with a peak at Nd and nearly flat patterns from Ta to Rb with troughs at Ba, Hf and deeper troughs at Zr and Pb. (Fig. 11A). The other clinopyroxenes show various patterns; two have REE patterns with an inflection in Eu and Gd and are similar in incompatible trace elements to garnets with deep Ba and Pb troughs. Two others show inflected or sinusoidal REE patterns with inflections in Gd and Dy and elevated incompatible elements with peaks in Nb and Pb (Fig. 11D).

All olivines have W-shaped REE patterns with abundances range from 1 to 0.01 relative to primitive mantle (PM) (McDonough and Sun, 1995) with local elevation near Gd and Tb. Most olivines show depressions in Ba, Sr, Y, Zr, Hf, Nb, Ta and a peak at Pb. Orthopyroxene shows a more enriched U-shaped REE near 0.1/PM and trace element spider diagram similar to those from mantle xenoliths from Bezymianny (Ionov et al., 2013) with peaks in Th, U, Hf and troughs or elevated Ta, Nb. Y. The only analyzed phlogopite (intergrowing with olivine) reveals peaks in Ba, Sr, Pb, elevated HFSE especially Zr but a trough in Y (Fig. 11D).

7.2 Trace elements in minerals from low-Cr suite

Ilmenite intergrowths with clinopyroxenes represent the low-Cr suite (Moore and Belousova, 2005). Clinopyroxenes from the intergrowths in general are similar to those of magmatic-type clinopyroxenes from lherzolites but some peaks in U and Ba. Trace element patterns in the ilmenites in intergrowths in general are nearly the same as those from megacrysts (Fig. 12A). They mostly have low abundances and W-shaped REE patterns with inflections in Gd and Eu, as in orthopyroxenes. In trace element spider diagrams they show peaks in Nb–Ta and Zr–Hf with smaller peaks in Pb but minima in Y. Two other enriched ilmenite grains demonstrate concave, inclined patterns in REE and elevated incompatible elements group but nearly the same levels in HFSE and without Y anomalies.

The trace element patterns for the minerals from the concentrates are in general very similar to those analyzed in xenoliths. But most of the clinopyroxenes belong to the low-Cr varieties and are closer to the high temperature Cpx from xenoliths and Ilm intergrowth and show patterns which are close to those from the associations described above (Fig. 12B).

8. Discussion

8.1. Comparison of P–T–X sections of Dalnyaya with other mantle columns beneath YKP

The mantle column beneath the Dalnyaya pipe shows some special features compared to those beneath other pipes in the Daldyn field. Garnet trends in the *P*–$Fe^{\#}$ diagram consist of several branches of increasing $Fe^{\#}$. Starting from the LAB at least four different levels occur in the mantle column, which may represent the traces of rising and differentiating melts. The deepest level (7–5.5 GPa) corresponds to the minimum effective viscosity of the mantle in the presence of melts (Karato, 2010) or water (Peslier, 2010) or an increase in oxygen fugacity, features which are commonly combined as a result of intrusion of protokimberlite melts (Goncharov et al., 2012; Doucet et al., 2014). Local shearing in the upper levels is also possible in the presence of melts and volatiles (Katayama et al., 2009). Possibly this took place in the mantle beneath Dalnyaya because deformed varieties yield rather high pressure ranges from >7 to 4.5 GPa.

Compared to the mantle sections beneath other large pipes in the Daldyn field such as Udachnaya and Zarnitsa, the Dalnyaya mantle section does not show the presence of eclogites and, even in the concentrates, orange eclogite-type garnets are not frequent.

The double *P*–CaO trend detected for garnets in Dalnyaya xenoliths, is most likely a sign of the reactions with Ca-rich melts, because Ca-riched varieties are typical for the high temperature varieties show signs of re-fertilization. The presence of sub-calcic garnets, which form several clots and trends in the lower part of the mantle section, suggests a rather high diamond grade of this pipe. The *P*–CaO trend for analyzed xenoliths with large amount of garnet and clinopyroxene is nearly constant within the 3–6 GPa interval, probably as a result of the influence of evolving melts. Evolving intergranular melts probably also had some influence. Pyroxenites showing most variability in compositions and TRE content are found mainly near the LAB and within the middle pyroxenite layer.

8.2 Trace elements evidence for mantle peridotite evolution

From trace element geochemistry, two major types of peridotites exist in the lithospheric mantle beneath Dalnyaya. The first group is characterized by negative anomalies in Ba, Sr, Pb

and sometimes Y and Nb–Ta. These features are found mainly in orthopyroxenes, some garnets and two clinopyroxenes. The other lithology corresponds to mantle that has interacted with plume-related melts, possibly protokimberlites. They are enriched in Ba, Sr and HFSE and have lower LILE concentrations. We tried to determine the tendencies of the changes of major and trace elements of different minerals in different levels of the mantle column.

Olivines show several trends of enrichments in Ti, Al, Ca vs Pressure (GPa), on the (Supplementary File 2, Fig.9A), which probably relates to the evolution of the melts with which they were in equilibrium. Greater enrichment of magma-related components occurs near the LAB.

Clinopyroxenes also show enrichment of Sr* ($Sr^*=\sqrt{Nd_n \times Sm_n}$), Pb, U/Pb, Zr and Y with slightly decreasing pressure. This may mean that reaction with the intruded melts occurred in 3 separate intervals probably corresponding to intermediate magma chambers for the protokimberlite melts. In the top of each interval corresponding to 6, 4.5 and 2.5 GPa, where melt concentration should be higher, the degree of interaction with wall-rock peridotites is also more intense. Increasing Ni in clinopyroxene shows the influence of ultramafic material or could also possibly be a result of contamination as happened with Cr in ilmenites (Fig. 10A of Supplementary File 2)

Garnets appear to have experienced major refertilization because their REE patterns are not harzburgitic. Only four of them show sinusoidal REE patterns and may be related to the primary type. There are correlations between the REE slope ($(La/Yb)_N$ or $(Gd/Yb)_N$ and values of Sr* minima or Y*, Pb*, which results from the decrease of the slope for the parental melts (Supplementary File 2, Fig. 10B) or degree of differentiation. The inclination of the HREE garnet slopes in the mantle column decreases with increasing temperature which is explained by mineral physics (Blundy and Wood, 1994). The degree of depletion is generally higher in the upper part of the mantle. But some characteristics of relatively depleted harzburgite associations are found for some garnets in the lower parts of the mantle.

The strong enrichment in the LILE components which commonly accompanies phlogopite and amphibole metasomatism (Gregoire et al., 2002) was not detected for most samples; only a few minerals in association with phlogopites show enrichment in Rb and Ba. However, most garnets show Nb–Ta enrichment similar to those from the Arkhangelsk kimberlite province (Afanasiev et al., 2013).

8.3. Reconstructed parental melts for minerals from xenoliths

The trace element compositions of melts reconstructed using K_D values (Hart and Dunn, 1993) for the main type of clinopyroxene related to refertilization almost completely coincide with those of the kimberlite melts from Dalnyaya pipe, having a gentle inclined pattern with Sr minimum (Kargin et al., 2011) and even a small Ta–Nb hump. Some clinopyroxenes reveal primary lherzolitic features in their more complex spider-diagrams and higher $(La/Yb)_N$ ratios. Formation of clinopyroxene in the sheared peridotites was caused by intrusion of protokimberlite melts, which produced megacrysts, porphyroclastic and sheared peridotites (Ionov et al., 2010; Agashev et al., 2013). Some peridotites with ovoid brecciated structures and veins with ilmenites and associated clinopyroxenes are possibly the first step in the formation of polymict breccias (Giuliani et al., 2013) (Fig. 13A).

The melts reconstructed from the garnets have different patterns depending on the partition coefficient used (Hauri, 1994; Harte and Kirkley, 1997; Green et al., 2000; Bedard, 2006; Tuff and Gibson, 2007; Fulmer et al., 2010; Girnis et al., 2013; Katzyura et al., 2015) (see Fig.8 of Supplementary File 2). If we use K_D for silicate melts (Green et al., 2000) which are lower in HFSE and LILE compared to those for carbonatite-silicate melts (Girnis et al., 2013; Katzyura et al., 2015), the obtained spider-diagrams show gently sloping patterns close to those obtained for the clinopyroxenes, except for the HFSE which are closer to those of kimberlites (Kargin et al., 2011).(Fig. 13C) Nevertheless the LREE for the clinopyroxene and garnet do not coincide entirely, nor do Ta–Nb and Zr–Hf; furthermore garnet shows much lower $(La/Sm)_N$ ratios than clinopyroxene, demonstrating incomplete equilibration. Resulting in trace element patterns almost completely coincide with clinopyroxene trace element spider-diagrams from Vitim mantle melts (Ashchepkov et al., 2011) which are also typical for plume melts formed by 1 % melting of garnet peridotites. $(La/Sm)_N$ deviations in garnet and clinopyroxene suggests that the melts which produced the garnets resulted from dissolution of primary clinopyroxenes. This "garnetization" may be caused by addition of water expanding the stability field of garnets and increasing pressure during ancient subduction.

The calculated melts for the olivines and orthopyroxene using partition coefficients after Imai et al. (2012) and Bedard (2006) show REE patterns which are inflected in Gd and are higher in LREE compared with melts in equilibrium with clinopyroxene (although this may result from uncertainty in partition coefficient; Fig. 13B). These inflected patterns are a common feature for most orthopyroxene from mantle xenoliths of Kamchatka (Ionov et al., 2013) and other xenolith localities in subduction settings (Ishimaru and Arai, 2009) and probably reflect a

primary subducted nature for the peridotites. These melts mostly have negative anomalies of Nd–Sm and Ta–Nb which are typical for subduction-related melts. However, U, Th and LILE contents are similar to orthopyroxene from peridotite xenoliths from Bezymianny (Ionov et al., 2013).

The reconstructed melts for the ilmenites estimated using K_D values of Zack and Brumm (1998) with addition for HFSE (Klemme et al., 2006) in general have very similar REE patterns to those determined for the megacrystic pyroxenites. But they are particularly high in HFSE and Pb. The depression from La to Sm cannot be explained by chromatographic effects but is more likely a result of selective removal of clinopyroxene from the rock, which may also explain the W-shaped pattern for the parental melts of olivine and orthopyroxene. Only two ilmenites show trace element multicomponent diagrams which resemble those of the host kimberlites (Kargin et al., 2011).

We checked the equilibrium of the garnet-clinopyroxene pair using the partition coefficients for clinopyroxene/garnet. In most cases they repeat the shapes of the K_D calculated for the garnet lherzolites and harzburgites from the Finsch pipe (Gibson et al., 2008), which were established to be equilibrated in trace elements and isotopic features (Lazarov et al., 2013). But those from Dalnyaya with close K_D in REE show some disequilibrium features such as the curved patterns in La–Nd and relative enrichment in the HFSE, which means that the parental melts were much closer to kimberlitic than those parental to the garnets (Fig. 14A). However, three K_D showing irregular patterns in REE diagrams related to clinopyroxene which was less enrich trace components which did not react with protokimberlites as those analyzed in SCLM beneath the Finsch pipe (Fig. 16 of Supplementary File 2).

Equilibrium between Cpx and Ilm in intergrowths is not complete. Only one sample (Dl175) shows a smooth partition coefficient pattern. We calculated the Ilm/melt partition. It shows higher values of the HFSE than those determined by Zack and Brumm (1998) with similar method for the Ilm-Cpx intergrowth from Hawaii cumulate basaltic xenoliths. However, the calculated parental melts for ilmenites are even less enriched in REE than with the previous K_D set (Fig. 14B).

8.4 Evolution of the melts in the mantle column beneath the Dalnyaya pipe

We suggest that the relic associations of garnet-clinopyroxene and especially the orthopyroxene with HFSE depressions may represent the ancient SCLM beneath the Daldyn

field. But they do not have positive anomalies at Pb, Sr and U which are the typical features of subduction-related fluid and melts, so they represent rather deep material which did not experience subduction.

Formation of the garnets with primitive round trace element patterns may be related to a refertilization probably associated with plume melts. This event was definitely prior to intrusion of the melts which created the shearing and metasomatism similar to processes in mantle column beneath Udachnaya pipe (Solov'ev et al., 2012; Kostrovitsky et al., 2013; Agashev et al., 2013). In general garnets and clinopyroxenes are essentially refertilized similar to the mantle beneath Finsch pipe (Lazarov et al., 2012). It seems that ultramafic melt equilibrated with the peridotites evidenced by the garnet and olivine from enriched refertilized peridotites having $Fe^{\#}$ = 0.09–0.10. Some pyroxenes may have been equilibrated with these garnets but most of them are more Fe-rich and closer to protokimberlites which, according to minerals from polymict breccias and sheared peridotites, have $Fe^{\#}$= 0.11–0.13. These large scale processes of interaction and refertilization have also been found in many kimberlite localities such as Udachnaya (Howarth et al., 2014; Pokhilenko et al., 2015) and are commonly associated with metasomatism by silicate-carbonatite melts.

It seems that this was the stage close to the formation of the channels through which the protokimberlite melt rose and in which megacrysts grew on the walls (Moore and Lock, 2002; Ashchepkov et al., 2014). This was followed by an increase of temperature and interaction with protokimberlite melts accompanied by an increase of Fe, Ca and Ti. The more Fe-rich varieties may represent samples of the low-Cr suite, which may be related to contact zones with the protokimberlite melt. Formation of ilmenites with depleted W-shaped REE patterns may be due to interaction of melts with rather depleted peridotite because melts commonly move through olivine-rich aggregates. Clinopyroxenes, olivine and one orthopyroxene found as inclusions in the ilmenite nodules are not the result of exsolution or pegmatoid intergrowth (Haggerty et al., 1975) but look like material captured by the kimberlite mush or later inflows of the protokimberlite melts. Thus, we can suggest a multistage evolution of the mantle beneath Dalnyaya pipe as was suggested for the Kaapvaal craton (Konzett et al., 2013).

8.5. Schemes of refertilization

The PTX diagrams show that refertilizing melts were intruded at several levels in the SCLM, at 6.5, 5.5 and 4.5 GPa according to clinopyroxene thermobarometry (Figs. 11 and 12).

529 The diagrams for the garnets show that they also occurred in the 3-2 GPa level. The changes of
530 characteristic ratios and incompatible elements from relatively fertile to more depleted in the
531 upper part of the mantle section suggest that refertilization originated in the asthenosphere. We
532 measured the garnets for trace elements mainly from the hot branch. The agents that caused
533 refertilization should be related to the last plume event. The question is why the garnets are not
534 equilibrated with the clinopyroxenes. It is likely that garnets were growing when the distant most
535 evolved melts with higher carbonatite fractions were interacting with the peridotites, dissolving
536 original orthopyroxenes and clinopyroxenes and thus they are richer in CaO than the garnets
537 from the low temperature branch (Fig. 12). In turn, clinopyroxenes with higher HREE than in
538 equilibrated peridotites from Finsch (Lazarov et al., 2013) should have dissolved some garnet
539 material. They grew later during increasing interaction near the developing channels and in many
540 cases show great compositional variations. A possible mechanism is that intruded melts were
541 rising the intergranular spaces, accompanied by differentiation (Burgess and Harte, 2004), i.e.,
542 assimilation fractionation crystallization (AFC) (De Paolo, 1984). This would be followed by an
543 increase of the incompatible elements together with the typical peridotitic components. The
544 second possibility is that the melts evolved in separate chambers and rose up step by step so that
545 the interaction took place mainly near the chambers and feeders.

546 The high temperature Fe-rich clinopyroxenes show an increase of Cr with decreasing
547 pressures. It is likely that that this is AFC with contamination of parental melts derived from
548 peridotites. But ilmenites which possibly crystallized from a separate liquid show a small
549 increase of Cr during ascent.

550 Modeling of AFC with different schemes (Fig. 15) including dissolution of garnets (or
551 clinopyroxene) and crystallization of clinopyroxenes (or garnet) or both together from partial
552 lherzolite melts (Ashchepkov et al., 2011) or kimberlite melts (Kargin et al., 2011) (Figs. 17–20
553 in Supplementary File 2) shows some similarities with the analyzed natural garnets and
554 clinopyroxenes (Fig. 14A, B, Fig. 15). Dissolution of clinopyroxene explains the bell-like REE
555 patterns for the garnets but cannot explain minima in HREE. Dissolution of garnet explains the
556 elevated HREE of clinopyroxene. Trace element components could be reduced by contamination
557 in orthopyroxenes and increase in HFSE content after ilmenite dissolution. It is possible to show
558 how the trace element components could be reduced by contamination in orthopyroxenes and
559 increasing HFSE content rises after ilmenite dissolution (Fig. 15D). Using uncontaminated
560 kimberlites compositions without HFSE anomalies (referring to melting degree F~1%) or partial
561 melts from primitive peridotites close to basalts (F~1 %) (Ashchepkov et al., 2011) can satisfy
562 the flat incompatible elements part of the original trace element compositions of garnets if we

use a K_D for silicate melts (e.g. Green et al., 2000). But using carbonatite-silicate melt coefficients (Girnis et al., 2013; Kazyura et al., 2015) produces elevated HFSE patterns. However, many garnet compositions show flat HREE minima from Ho to Yb which could be derived from the original depleted source. It is necessary to melt a major amount of orthopyroxenes or another mineral to form U-shaped HREE pattern. Orthopyroxene melting is a common model for silica enrichment of carbonatitic kimberlite melts (Brett et al., 2015).

8.6. Significance of melt interaction for diamond grade

The relatively low diamond grade of the Dalnyaya pipe could be the result of several processes. First is the high degree of mantle metasomatism by highly oxidized melts. This is visible also in the NS mantle transect (Fig. 21 in Supplementary File 2) of the SCLM from the Daldyn field. Nearly half of the clinopyroxenes from xenoliths fall outside the diamond stability field in the *P*-fO_2 diagrams, together with the ilmenites. The very low concentration of eclogites and pyroxenites is also an unfavorable factor because nearly half of the diamonds in productive kimberlites belong to the eclogite type, according to their inclusions (Sobolev et al., 2004; Logvinova et al., 2005). The amount of sub-calcic garnets, which probably were produced by percolation of reduced fluid in Archean time (Klein-Ben David et al., 2014) within the dunite channels (Pearson and Wittig, 2014), is also relatively low compared to the other large pipes.

9. Conclusions

(1) The peridotite mantle beneath the Dalnyaya pipe underwent multistage metasomatism and, was affected by oxidized melts related to protokimberlites during the final stage;

(2) Many mineral associations in the mantle column are not thermally and chemically equilibrated;

(3). The lithospheric mantle beneath the Dalnyaya pipe is layered and consists of five stepped layers which were heated to different degrees;

(4). The SCLM beneath Dalnyaya contains very small amounts of eclogites and pyroxenites and originally was built up by peridotites which could be island arc-type, but lack the signs of U, Sr, Ba subduction-related metasomatism.

Acknowledgements

We are very thankful to ALROSA Company for help in sampling. Many thanks to S.V. Palessky for the performing of the LA-ICP-MS measurements and to O.S. Khmelnikova for help in microprobe measurements on Camebax Micro in Analytic Centre IGM SB RAS. The works are supported by RBRF grants: 05-05-64718, 11-05-00060; 11-05-91060-PICS; 16-05-00860. The work contains the result of the projects 77-2, 65-03, 02-05 UIGGM SD RAS and ALROSA Stock Company.

References

Afanasiev, V.P., Ashchepkov, I.V., Verzhak, V.V., O' Brien, H., Palessky, S.V., 2013. PT conditions and trace element variations of picroilmenites and pyropes from the Arkhangelsk region. Journal of Asian Earth Sciences 70, 45-63.

Agashev A.M., Pokhilenko N.P., Tolstov A.V., Polyanichko N.P., Mal'kovets V.G., Sobolev N.V., 2004. New data on age of kimberlites from Yakutian kimberlite province. Doklady Earth sciences RAN 399, 95–99.

Agashev, A. M., Ionov, D. A., Pokhilenko, N. P., Golovin, A. V., Cherepanova,Yu, Sharygin, I. S., 2013. Metasomatism in lithospheric mantle roots: Constraints from whole-rock and mineral chemical composition of deformed peridotite xenoliths from kimberlite pipe Udachnaya. Lithos 160, 201-215.

Amshinsky, A.N., Pokhilenko, N.P., 1983. Peculiarities of the pycroilmenite compositions from Zarnitsa kimberlite pipe (Yakutia). Russian Geology and Geophysics 24 (11), 116-119.

Arndt, N.T., Guitreau, M., Boullier, A.-M. leRoex, A., Tommasi, A., Cordier, P., Sobolev A., 2010. Olivine, and the origin of kimberlite. Journl of Petrology 51 (3), 573–602.

Ashchepkov, I.V., Pokhilenko, N.P., Vladykin, N.V., Logvinova, A.M., Kostrovitsky, S.I., Afanasiev, V.P., Pokhilenko, L.N., , Kuligin, S.S., Malygina, L.V., Alymova, N.V., Khmelnikova, O.S., Palessky, S.V., Nikolaeva, I.V., Karpenko, M.A., Stagnitsky, Y.B., 2010. Structure and evolution of the lithospheric mantle beneath Siberian craton, thermobarometric study. Tectonophysics 485, 17-41.

Ashchepkov, I.V., André, L., Downes, H., Belyatsky, B.A., 2011. Pyroxenites and megacrysts from Vitim picrite-basalts (Russia): Polybaric fractionation of rising melts in the mantle? Journal of Asian Earth Sciences 42, 14-37.

Ashchepkov, I.V., Rotman, A.Y., Somov, S.V., Afanasiev, V.P., Downes, H., Logvinova,

626 A.M., Nossyko, S. Shimupi, J., Palessky, S.V., Khmelnikova, O.S., Vladykin, N.V., 2012.
627 Composition and thermal structure of the lithospheric mantle beneath kimberlite pipes from the
628 Catoca cluster, Angola. Tectonophysics 530, 128-151
629 Ashchepkov, I.V., Vladykin, N.V., Ntaflos, T., Downes, H., Mitchel, R., Smelov, A.P.
630 Rotman,A.Ya., Stegnitsky, Yu., Smarov, G.P, Makovchuk, I.V., Nigmatulina, E.N.,
631 Khmelnikova, O.S., 2013a. Regularities of the mantle lithosphere structure and formation
632 beneath Siberian craton in comparison with other cratons. Gondwana Research 23, 4-24.
633 Ashchepkov, I.V., Ntaflos, T., Kuligin, S.S., Malygina, E.V., Agashev, A.M., Logvinova,
634 A.M., Mityukhin, S.I., Alymova, N.V., Vladykin, N.V., Palessky, S.V., Khmelnikova, O.S.,
635 2013b. Deep-Seated Xenoliths from the Brown Breccia of the Udachnaya Pipe, Siberia. D. G.
636 Pearson et al. (eds.). Proceedings of 10th International Kimberlite Conference. - New Delhi:
637 Springer India, v. 1., 59-74.
638 Ashchepkov, I.V., Downes, H., Mitchell, R., Vladykin, N.V., Coopersmith, H., Palessky,
639 S.V., 2013c. Wyoming Craton Mantle Lithosphere: Reconstructions Based on Xenocrysts from
640 Sloan and Kelsey Lake Kimberlites. In: Pearson D. G. et al. (eds.) Proceedings of 10th
641 International Kimberlite Conference. - New Delhi: Springer India, v. 1. 13-27
642 Ashchepkov I.V., Vladykin N.N., Ntaflos T., Kostrovitsky S.I., Prokopiev S.A., Downes
643 H., Smelov A.P., Agashev A.M., Logvinova A.M., Kuligin S.S., Tychkov N.S., Salikhov R.F.,
644 StegnitskyYu.B., Alymova N.V., Vavilov M.A., Minin V.A., Babushkina S.A.,
645 OvchinnikovYu.I., Karpenko M.A., Tolstov A.V., Shmarov G.P., 2014a. Layering of the
646 lithospheric mantle beneath the Siberian Craton: Modeling using thermobarometry of mantle
647 xenolith and xenocrysts Tectonophysics 634, 55-75.
648 Ashchepkov I. V. , Alymova N. V., Logvinova A. M., Vladykin N. V., Kuligin S. S.,
649 Mityukhin S. I., Downes H., Stegnitsky Yu. B., Prokopiev S.A., Salikhov R.F., Palessky V. S.,
650 Khmel'nikova O. S., 2014b. Picroilmenites in Yakutian kimberlites: variations and genetic
651 models. Solid Earth 5, 915-938.
652
653 Ashchepkov, I.V., Logvinova, A.M., Reimers, L.F., Ntaflos, T., Spetsius, Z.V., Vladykin,
654 N.V., Downes, H., Yudin, D.S., Travin, A.V., Makovchuk, I.V. and Palesskiy, V.S., 2015. The
655 Sytykanskaya kimberlite pipe: Evidence from deep-seated xenoliths and xenocrysts for the
656 evolution of the mantle beneath Alakit, Yakutia, Russia. *Geoscience Frontiers 6*(5), 687-714.
657 Ashchepkov I, Logvinova A, Spetsius Z andStegnitsky Y., 2015. Monomineral Mantle
658 Elcogite CPx and Garnet Thermobarometry. Goldschmidt 2015 Abstracts. A126.
659 Bedard, J. H., 2006. A catalytic delamination-driven model for coupled genesis of
660 Archaean crust and sub-continental lithospheric mantle. Geochimica et Cosmochimica Acta 70,

1188 -1214..

Blundy, J., Wood, B., 1994. Prediction of crystal-melt partition-coefficients from elastic-moduli. Nature 372, 452–454.

Bussweiler, Y., Foley, S.F., Prelević, D., Jacob D.E., 2015. The olivine macrocryst problem: New insights from minor and trace element. Lithos 220, 238-252.

Boyd, F.R., Pokhilenko, N.P., Pearson, D.G., Mertzman S.A., Sobolev, N.V., Finger, L.W., 1997. Composition of the Siberian cratonic mantle: evidence from Udachnaya peridotite xenoliths. Contributions Mineralogy and Petrology 128, 228-246.

Boyd, F.R., 1973. A pyroxene geotherm. Geochimica et Cosmochimica Acta 37, 2533-2546.

Brett, R.C., Russell, J.K., Andrews, G.D.M., Jones, T.J., 2015. The ascent of kimberlite: Insights from olivine. Earth and Planetary Science Letters 424, 119–131.

Burgess, S.R., Harte, B., 2004. Tracing lithosphere evolution through the analysis of heterogeneous G9-G10 garnets in peridotite xenoliths, II: REE chemistry.Journal of Petrology 45, 609-634.

Brey, G.P., Kohler, T., 1990.Geothermobarometry in four-phase lherzolites. II. New thermobarometers, and practical assessment of existing thermobarometers. Journal of Petrology 31, 1353-1378.

Bussweiler, B., Foley, S.F., Prelević, D., Jacob, D.E., 2014. The olivine macrocryst problem: New insights from minor and trace element compositions of olivine from Lac de Gras kimberlites, Canada. Lithos 220, 238–252.

Cas, R.A.F., Porritt, L., Pittari, A., Hayman, P.C., 2008. A new approach to kimberlite terminology using a revised general approach to the nomenclature of all volcanic rocks and deposits: descriptive to genetic. J. Volcanol. Journal of Volcanology and Geothermal Researc 174, 226–240.

Clarke, D.B., Mackay, R.M., 1990. An Ilmenite-Garnet-Clinopyroxene nodule from Matsoku: Evidence of Oxide-Rich liquid Immiscibility in Kimberlites? Canadian Mineralogist 28, 229-239.

Day H.W., 2012. A revised diamond-graphite transition curve. American Mineralogist, 97, 52–62.

DePaolo D.J., 1981. Trace element and isotopic effects of combined wall rock assimilation and fractional crystallization. Earth Planetary Science Letters 53, 189-202.

Doucet, L. S.,Peslier, A.H., Ionov, D.A., Brandon, A.D., Golovin, A.V., Goncharov, A.G., Ashchepkov, I.V., 2014. High water contents in the Siberian cratonic mantle linked to

metasomatism: An FTIR study of Udachnaya peridotite xenoliths. Geochimica et Cosmochimica Acta 137, 159-187.

Evans, T.M., O'Neill, C., Tuff, H. St, J., 2008. The influence of melt composition on the partitioning of REEs, Y, Sc, Zr and Al between forsterite and melt in the system CMAS. Geochim. Cosmochim. Acta 72, 5708–5721.

Finnerty, A.A., Boyd, F.R. 1984. Evaluation of thermobarometers for garnet peridotites Geochimica et Cosmochimica Acta, 48, 15–27.

Foley, S.F., Yaxley, G.M., Rosenthal, A., Buhre, S., Kiseeva, E.S., Rapp, R.P., Jacob, D.E., 2009. The composition of near-solidus melts of peridotite in the presence of CO2 and H2O between 40 and 60 kbar. Lithos 112, 274-283.

Fulmer, E.C., Nebel, OP., van Westrenen E., 2010. High-precision high field strength element partitioning between garnet, amphibole and alkaline melt from Kakanui, New Zealand. Geochimica et Cosmochimica Acta 74, 2741-2759.

Genshaft, Yu.S.,Ilupin, I.P., 1987. Deep Seated Paragenesis of Ilmenite In The Kimberlite of Yakutia. In: Studies of Ultra-Basic Minerals. Moscow. IFZ OF AS USSR.25-68 (in Russian).

Gibson, S.A., Malarkey, J., Day, J.A., 2008. Melt depletion and enrichment beneath the western Kaapvaal Craton: evidence from Finsch peridotite xenoliths. Journal of Petrology 49, 1817–1852.

Goncharov, A. G., Ionov, D. A., Doucet, L. S., Pokhilenko, L. N., 2012. Thermal state, oxygen fugacity and C-O-H fluid speciation in cratonic lithospheric mantle: New data on peridotite xenoliths from the Udachnaya kimberlite, Siberia. Earth and Planetary Science Letters 357, 99-110.

Gregoire, M., Bell, D. R., Le Roex, A. P., 2002.Trace element geochemistry of phlogopite-rich mafic mantle xenoliths: their classificationand their relationship to phlogopite-bearing peridotites and kimberlites revisited. Contributions to Mineralogy and Petrology 142, 603 -625.

Green, T.H., Blundy, J.D., Adam, J., Yaxley., G.M., 2000. SIMS determination of trace element partition coefficients between garnet, clinopyroxene and hydrous basaltic liquids at 2–7.5 GPa and 1080–1200°C. Lithos 53, 165-187.

Griffin, W. L., Ryan, C. G., Kaminsky, F. V., O'Reilly, S. Y., Natapov, L. M., Win, T. T., Kinny, P.D., Ilupin, I. P., 1999a. The Siberian lithosphere traverse: Mantle terranes and the assembly of the Siberian Craton. Tectonophysics 310, 1-35.

Griffin, W. L., O'Reilly, S.Y., Afonso, J.C., Begg, G.C., 2009. The Composition and

729 Evolution of Lithospheric Mantle: A Reevaluation and Its Tectonic Implications, Journal of
730 Petrology 50, 1185–1204
731 Griffin, W.L., Spetsius, Z.V., Pearson, N.J., O'Reilly, S.Y. 2002. In-situ Re-Os analysis
732 of sulfide inclusions in kimberlite olivine: New constraints on depletion events in the Siberian
733 lithospheric mantle. Geochemistry, Geophysics, Geosystems, 3, (11), 1069,
734 doi:10.1029/2001GC000287.
735 Haggerty, S.E.1975. The chemistry and genesis of opaque minerals in kimberlite. Physics
736 and chemistry of the Earth. New York 9, 227-243.
737 Hammouda, T.,Keshav, S. 2015. Melting in the mantle in the presence of carbon: Review
738 of experiments and discussion on the origin of carbonatites. Chemical Geology 418, 171-188.
739 Hart, S. R., Dunn, T., 1993. Experimental cpx/melt partitioning of 24 trace elements.
740 Contributions to Mineralogy and Petrology 113, 1-8.
741 Harte, B., Kirkley, M.B., 1997. Partitioning of trace elements between clinopyroxene and
742 garnet: data from mantle eclogites. Chemical Geology 136, 1-24.
743 Hauri, E.H., Wagner, T.P., Grove, T.L., 1994. Experimental and natural partitioning of
744 Th, U, Pb and other trace elements between garnet, clinopyroxene and basaltic melts. Chemical
745 Geology 117, 149–166.
746 Höfer, H.E., Lazarov, M., Brey, G.P., Woodland, A.B., 2009. Oxygen fugacity of the
747 metasomatizing melt in a polymict peridotite from Kimberley. Lithos 112S, 1150–1154
748 Giuliani, A., Kamenetsky, V.S., Kendrick, M.A., Phillips, D., Wyatt, B.A., Maas, R.,
749 2013. Oxide, sulphide and carbonate minerals in a mantle polymict breccia: Metasomatism by
750 proto-kimberlite magmas, and relationship to the kimberlite megacrystic suite. Chemical
751 Geology, 353, 4-18.
752 Howarth, G.,H. Barry,P.H,. Pernet-Fisher, J.F.,Baziotis,I. P., Pokhilenko,N.P.,
753 Pokhilenko, L.N.,Bodnar,R.J., Taylor, L.A., Agashev A.M., 2014. Superplume metasomatism:
754 Evidence from Siberian mantle xenoliths. Lithos 184–187, 209-224.
755 Horn, I., Foley,S.F.,Jackson, S.E., Jenner,G.A., 1994.Experimentally determined
756 partitioning of high field strength- and selected transition elements between spinel and basaltic
757 melt. Chemical Geology117, 193–218.
758 New Diamond Fields Explored by ALROSA May Turn Into Possible Sources of Reserve
759 Growth. Experet reports -2012. In: Rough and Polished, http://www.rough-
760 polished.com/en/expertise/61434.html
761 Ionov, D.A., Doucet, L.S., Ashchepkov I.V. 2010. Composition of the Lithospheric
762 Mantle in the Siberian Craton: New Constraints from Fresh Peridotites in the Udachnaya-East
763 Kimberlite. Journal of Petrology 51, 2177-2210.

Ionov, D.A., Bénard, A., Plechov, P.Yu., Shcherbakov, V.D., 2013. Along-arc variations in lithospheric mantle compositions in Kamchatka, Russia: First trace element data on mantle xenoliths from the Klyuchevskoy Group volcanoes. Journal of Volcanology and Geothermal Research 263, 122–131.

Ishimaru ,S., Arai, S., 2009. Highly silicic glasses in peridotite xenoliths from Avacha volcano, Kamchatka arc; implications for melting and metasomatism within the sub-arc mantle. Lithos 107, 93–106.

Imai, T., Takahashia, E., Suzuki, T., Hirata, T., 2012. Element partitioning between olivine and melt up to 10 GPa: Implications for the effect of pressure. Physics of the Earth and Planetary Interiors 212, 64–75.

Karato, S., 2010. Rheology of the Earth's mantle: A historical review. Gondwana Research 18, 17–45.

Kargin, A.V., Golubeva, Yu.Yu.,Kononova V.A., 2011. Kimberlites of the Daldyn-Alakit region (Yakutia): Spatial distribution of the rocks with different chemical characteristics. Petrology. 19 (5), 496–520.

Katayama, I., Suyama, Y., Ando, S., Komiya, T., 2009. Mineral chemistry and P–T condition of granular and sheared peridotite xenoliths from Kimberley, South Africa: origin of the textural variation in the cratonic mantle. Lithos 109, 333–340.

Kuzyura, A.V., Litvin, Yu.A., Jeffries, T., 2015. Interface partition coefficients of trace elements in carbonate–silicate parental media for diamonds and paragenetic inclusions (experiments at 7.0–8.5 GPa). Russian Geology and Geophysics56, 221–231.

Khar'kiv, A.D., Zinchuk, N.N., and Kryuchkov, A.I., 1998. Korennye mestorozhdeniya almazov mira (Primary diamond deposits of the world), Moscow: Nedra.

Kennedy, C.S., Kennedy, G.C., 1976. The equilibrium boundary between graphite and diamond. Journal of Geophysical Research 81, 2467–2470.

Klein-Ben David, O., Pearson, D.G.., Nowell G.M., Ottley C., McNeill, J.C.R., Logvinova, A., Sobolev, N.V., 2014. The sources and time-integrated evolution of diamond-forming fluids – Trace elements and isotopic evidence. Geochimica et Cosmochimica Acta 125, 146–169.

Klemme, S., Günther, D., Hametner, K., Prowatke, S., Zack, T., 2006. The partitioning of trace elements between ilmenite, ulvospinel, armalcolite and silicate melts with implications for the early differentiation of the moon. Chemical Geology 234, 251–263.

Kohler, Brey G.P., 1990. Calcium exchange between olivine and clinopyroxene calibrated as a geothermobarometerfor natural peridotites from 2 to 60 kb with applications. Geochemicaet Cosmochimica Acta. 54, 2375–2388.

Konzett,Y., Wirth, R., Hauzenberger, K., Whitehouse, M., 2013.Two episodes of fluid migration in the Kaapvaal Craton lithospheric mantle associated with Cretaceous kimberlite activity: Evidence from a harzburgite containing a unique assemblage of metasomatic zirconium-phases. Lithos 182, 65–184.

Kopylova, M. G., Nowell, G. M., Pearson, D. G., Markovic, G., 2009. Crystallization of megacrysts from protokimberlitic fluids: Geochemical evidence from high-Cr megacrysts in the Jericho kimberlite. Lithos 112, 284–295.

Kostrovitsky,S. I., Solov'eva,L.V., Yakovlev,D.A.,Suvorova, L.F., Sandimirova, G.P., Travin,A.V.,Yudin, D. S., 2013. Kimberlites and megacrystic suite: Isotope-geochemical studies. Petrology 21 (2), 127–144.

Kuzyura, A.V., Litvin, Yu.A., Jeffries, T., 2015. Interface partition coefficients of trace elements in carbonate-silicate parental media for diamonds and paragenetic inclusions (experiments at 7.0-8.5 GPa). Russian Geology and Geophysics 56, 221–231.

Lavrent'ev, Yu.G., Usova, L.V., Kuznetsova, A.I., Letov, S.V., 1987. X-ray spectral quant metric microanalysis of the most important minerals of kimberlites Russian Geology and Geophysics, 48 (5), 75–81.

Logvinova, A.M., Taylor, L.A., Floss, C., Sobolev, N.V., 2005.Geochemistry of multiple diamond inclusions of harzburgitic garnets as examined in situ. International Geology Review 47, 1223–1233.

Lavrent'ev, Yu.G., Usova, L.V., Kuznetsova, A.I., Letov, S.V., 1987. X-ray spectral quantimetric microanalysis of the most important minerals of kimberlites. Russian Geology and Geophysics 48 (5), 75–81.

Lazarov, M., Brey, G. P., Stefan Weyer, S., 2012. Evolution of the South African mantle — A case study of garnet peridotites from the Finsch diamond mine (Kaapvaal craton); part 1: Inter-mineral trace element and isotopic equilibrium. Lithos 154, 193–209.

Laz'ko E.E., Roden M. F., 2003. Garnet Peridotites and Pyroxenites in The Subcontinental Lithosphere of the Central Part of Siberian Craton (Xenoliths From The Mir Pipe) Problems of Prediction, Prospection and Investigation of the Deposits of the Ore and Mineral Resources at the Boundary of XXI Century. Voronezh.. Voronezh State University. pp. 307–317 (in Russian)

Logvinova, A.M., Taylor, L.A., Floss, C., Sobolev, N.V., 2005. Geochemistry of multiple diamond inclusions of harzburgitic garnets as examined in situ. International Geology Review 47, 1223–1233.

McCammon, C.A., Griffin, W.L., Shee, S.R., O'Neill, H.S.C., 2001. Oxidation during metasomatism in ultramafic xenoliths from the Wesselton kimberlite, South Africa: implications

for the survival of diamond. Contributions Mineralogy and Petrology 141, 287–296.

McCammon, C.A., Kopylova, M.G., 2004. A redox profile of the Slave mantle and oxygen fugacity control in the cratonic mantle. Contributions to Mineralogy and Petrology 148, 55–668.

McDonough, W.F., Sun, S.-S., 1995.The composition of the Earth. Chemical Geology 120, 223–253.

Mitchell, R.H., 1995. Kimberlites, Orangeites and Related Rocks. Plenum Press, New York. 410 pp.

McGregor I.D.,1974. The system MgO- SiO_2-Al_2O_3: solubility of Al_2O_3 in enstatite for spinel and garnet peridotite compositions. American Mineralogist 59, 110–119.

Moore, A.E., Lock, N.P., 2001. The origin of mantle-derived megacrysts and sheared peridotitesevidence from kimberlites in the northern Lesotho—Orange Free State (South Africa) and Botswana pipe clusters. South Africa Journal of Geology 104, 23–38.

Moore, A., Belousova, E., 2005. Crystallization of Cr-poor and Cr-rich megacryst suites fromthe host kimberlite magma: implications for mantle structure and the generation of kimberlite magmas. Contributions to Mineralogy and Petrology 49, 462–481.

Nickel, K.G., 1989. Garnet-pyroxene Equilibria in the System SMACCR (SiO_2-MgO-Al_2O_3-CaO-Cr_2O_3): the Cr-geobarometer. In Ross, J. (ed.): Kimberlites and Related Rocks, Their Mantle/Crust Setting, Diamonds and Diamond Exploration. Vol.2. Proc. 4th Int. Kimberlite Conf. /Geol. Soc. Aus. Spec. Publ., 14, 901–912.

Nimis P., Taylor W., 2000. Single clinopyroxene thermobarometry for garnet peridotites. Part I. Calibration and testing of a Cr-in-Cpx barometer and an enstatite-in-Cpx thermometer. Contributions to Mineralogy and Petrology 139, 541–554.

Nimis P., Zanetti A., Dencker I., Sobolev N.V., 2009. Major and trace element composition of chromian diopsides from the Zagadochnaya kimberlite (Yakutia, Russia): Metasomatic processes, thermobarometry and diamond potential. Lithos 112, 397–412.

O'Neill, H. St. C., Wall, V. J., 1987. The olivine orthopyroxene-spinel oxygen geobarometer, the nickel precipitation curve, and the oxygen fugacity of the Earth's upper mantle. Journal of Petrology 28, 1169–1191.

O'Neill, H.St.C, Wood B.J., 1979. An experimental study of Fe-Mg- partitioning between garnet and olivine and its calibration as a geothermometer. Contributions to Mineralogy and Petrology 70, 59–70.

Pearson, D.G. and Wittig, N., 2014. The formation and evolution of cratonic mantle lithosphere—Evidence from mantle xenoliths. *Treatise on Geochemistry 2*, 255-292.

Pernet-Fisher, J.F., Howarth, G.H., Liu, Y., Barry, P.H., Carmody, L., Valley, J.W., Bodnar, R.J., Spetsius, Z.V., Taylor L.A., 2014. Komsomolskaya diamondiferous eclogites: evidence for oceanic crustal protoliths. Contributions to Mineralogy and Petrology 167, 1–17.

Peslier, A.H., Woodland, A.B., Bell, D. R., Lazarov, M., 2010. Olivine water contents in the continental lithosphere and the longevity of cratons. Nature 467, 78–81.

Pokhilenko, N. P., Sobolev, N.V., Kuligin, S. S., Shimizu, N., 1999. Peculiarities of distribution of pyroxenite paragenesis garnets in Yakutian kimberlites and some aspects of the evolution of the Siberian craton lithospheric mantle. Proceedings of the VII International Kimberlite Conference. The P.H. Nixon volume. 690–707.

Pokhilenko, N.P., Pearson, D.G., Boyd, F.R., Sobolev, N.V., 1991. Megacrystalline dunites: sources of Siberian diamonds. Carnegie Institute Washington. Yearbook 90, 11–18.

Pokhilenko, N. P., Sobolev, N.V., Kuligin, S. S., Shimizu, N., 1999. Peculiarities of distribution of pyroxenite paragenesis garnets in Yakutian kimberlites and some aspects of the evolution of the Siberian craton lithospheric mantle. Proceedings of the VII International Kimberlite Conference. The P.H. Nixon volume. 690–707.

Pokhilenko, N. P., Sobolev N.V., Sobolev V.S. and Lavrentiev Y.G., 1976. Xenoliths of diamond bearing ilmenite-pyrope lherzolites from the kimberlite pipe Udachnaya (Yakutia). Doklady AN SSSR.. 231, 438–442.

Pokhilenko, N.P., Agashev, A.M., Litasov, K.D., Pokhilenko, L.N., 2015. Carbonatite metasomatism of peridotite lithospheric mantle: implications for diamond formation and carbonatite-kimberlite magmatism. Russian Geology and Geophysics 56, 280–295.

Rodionov, A.S., Amshinsky A.N., Pokhilenko, N P., 1988. Ilmenite – Pyrope wehrlite – are the new type of paragenesisin xenoliths fromkimberlite. Russian Geol. Geophys. 19/7, 53–57.

Rodionov, A S., Amshinsky., Pokhilenko, N P., Sobolev, N.V., 1984. Comparative description of the mainminerals in the concentrate of two varieties of kimberlites in Dal'nyaya pipe (Yakutia). Russian Geol. Geophys. 17, 38–50.

Rodionov, A.S., Sobolev, N.V., Pokhilenko, N.P., Suddaby, P., Amshinsky, A.N., 1991. Ilmenite-bearing peridotites and megacrysts from Dalnyaya kimberlite pipe, Yakutia. Fifth International Kimberlite Conference: Extended abstracts, United States, 339–341.

Rudnick, R.L., McDonough, W.F., O'Connell R.J., 1998. Thermal structure, thickness and composition of continental lithosphere. Chemical Geology 145, 395–411.

Sazonova, L.V., Nosova, A.A., Kargin, A.V., Borisovskiy, S.E., Tretyachenko, V.V., Abazova, Z.M., Griban' Yu.G., 2015. Olivine from the Pionerskaya and V. Grib kimberlite

902 pipes, Arkhangelsk diamond province, Russia: Types, composition, and origin. Petrology 23,
903 227–258.
904 Smelov, A.P., Zaitsev, A.I., 2013. The Age and Localization of Kimberlite Magmatism in
905 the Yakutian Kimberlite Province: Constraints from Isotope Geochronology—An Overview.
906 Pearson D. G. et al. (eds.), Proceedings of 10th International Kimberlite Conference, Volume 1,
907 Special Issue of the Journal of the Geological Society of India, 225–234.
908 Sobolev, N.V., Lavrent'ev, Y.G., Pokhilenko, N.P., Usova, L.V., 1973. Chrome-Rich
909 Garnets from the Kimberlites of Yakutia and Their Parageneses. Contributions to Mineralogy
910 and Petrology 40, 39–52.
911 Sobolev, N.V., Logvinova, A.M., Zedgenizov, D.A., Pokhilenko, N.P., Malygina, E.V.,
912 Kuzmin, D.V., Sobolev, A.V., 2009. Petrogenetic significance of minor elements in olivines
913 from diamonds and peridotite xenoliths from kimberlites of Yakutia. Lithos, 112S1, 701–713.
914 Sobolev, N.V., Sobolev, A.V., Tomilenko, A.A., Kovyazin, S.V., Batanova, V.G.,
915 Kuz'min, D.V., 2015. Paragenesis and complex zoning of olivine macrocrysts from unaltered
916 kimberlite of the Udachnaya-East pipe, Yakutia: relationship with the kimberlite formation
917 conditions and evolution. Russian Geology and Geophysics 56, 260–279.
918 Sobolev, N.V., 1977. Deep-Seated Inclusions in Kimberlites and the Problem of the
919 Composition of the Mantle. Amer. Geophys. Union, Washington, DC. 279 pp.
920 Sobolev, N.V., Pokhilenko, N.V., Efimova, E.S., 1984. Xenoliths of diamond bearing
921 peridotites in kimberlites and problem of the diamond origin. Russian Geology and Geophysics,
922 25, 63–80.
923
924 Sobolev, N.V., Logvinova, A.M., Zedgenizov, D.A., Pokhilenko, N.P., Malygina, E.V.,
925 Kuzmin, D.V., Sobolev, A.V., 2009. Petrogenetic significance of minor elements in olivines
926 from diamonds and peridotite xenoliths from kimberlites of Yakutia. Lithos, 112, 701-713.
927 Sobolev N.V., Kuznetsova, I.K., Zyuzin, N.I., 1968. The petrology of grospydite
928 xenoliths from the Zagadochnaya kimberlite pipe in Yakutia. Journal of Petrology 9, 253–280.
929 Solov'eva, L.V., Yasnygina,T.A., Egorov K.N., 2012. Metasomatic parageneses in deep-
930 seated xenoliths from pipes Udachnaya and Komsomol'skaya-Magnitnaya as indicators of fluid
931 transfer through the mantle lithosphere of the Siberian craton. Russian Geology and Geophysics
932 53, 1304–1323.
933 Sobolev N.V., Kuznetsova, I.K., Zyuzin, N.I., 1968. The petrology of grospydite
934 xenoliths from the Zagadochnaya kimberlite pipe in Yakutia. Journal of Petrology 9, 253–280.

Spetsius, Z.V., 2007. The nature of indicator minerals in kimberlites: a case from the mantle xenoliths studying. Plumes and their sources. Ed. by N.V. Vladykin. Irkutsk. Institute of Geography, 90–108.

Spetsius, Z.V., Serenko, V.P., 1990. Composition of the Continental Mantle and Low Crust Beneath the Siberian Platform. Moscow, Nauka. 271 pp (in Russian).

Stachel, T., Luth, R.W., 2015. Diamond formation — Where, when and how? Lithos 220, 200–220.

Stagno, V. Frost, D.J., 2010. Carbon speciation in the asthenosphere: experimental measurements of the redox conditions at which carbonate - bearing melts coexist with graphite or diamond in peridotite assemblages. Earth Planetary Science Letters 300, 72–84,

Stagno, V., Ojwang, D.O., McCammon, C.A. Frost, D.J., 2013. The oxidation state of the mantle and the extraction of carbon from Earth's interior. Nature 493, 84–88.

Sun, C., Liang, Y., 2015. A REE-in-garnet–clinopyroxene thermobarometer for eclogites, granulites and garnet peridotites. Chemical Geology 393, 79–92.

Tappe, S., Pearson, D.G., Kjarsgaard, B.A., Nowell, G., Dowall, D., 2013. Mantle transition zone input to kimberlite magmatism near a subduction zone: Origin of anomalous Nd–Hf isotope systematics at Lac de Gras, Canada. Earth and Planetary Science Letters 371, 235–251.

Taylor, W.R., Kammerman, M., Hamilton, R., 1998. New thermometer and oxygen fugacity sensor calibrations for ilmenite and chromian spinel-bearing peridotitic assemblages.7th International Kimberlite Conference. Extended abstracts. Cape Town. 891–901

Tappe, S., Pearson, D.G., Kjarsgaard, B.A., Nowell, G., Dowall, D., 2013. Mantle transition zone input to kimberlite magmatism near a subduction zone: Origin of anomalous Nd–Hf isotope systematics at Lac de Gras, Canada. Earth and Planetary Science Letters 371, 235–251.

Taylor, W.R., Kammerman, M., Hamilton, R.1998. New thermometer and oxygen fugacity sensor calibrations for ilmenite and chromian spinel-bearing peridotitic assemblages.7th International Kimberlite Conference. Extended abstracts. Cape Town. 891–901

Tappe, S., Foley, S.F., Jenner, G.A., Heaman L.M., Kjarsgaard B. A., Romer R. L., Stracke A., Joyce N., Hoefs J., 2006. Genesis of ultramafic lamprophyres and carbonatites at Aillik Bay, Labrador: a consequence of incipient lithospheric thinning beneath the North Atlantic craton Journal of Petrology 47, 1261–1315.

Tuff, J., Gibson, S., 2007. Trace-element partitioning between garnet, clinopyroxene and FE-rich picritic melts at 3 to 7 Gpa. Contributions to Mineralogy and Petrology 153, 369–387.

Walter, M.J., 1998. Melting of Garnet Peridotite and the Origin of Komatiite and Depleted Lithosphere. Journal of Petrology 39, 29–60.

Wang, H., van Hunen, J., Pearson, D.G., 2015. The thinning of subcontinental lithosphere: The roles of plume impact and metasomatic weakening. Geochemistry, Geophysics, Geosystems 16(4), 1156-1171.

Wu, C.-M., Zhao, G., 2011. The applicability of garnet–orthopyroxene geobarometry in mantle xenoliths. Lithos 125, 1–9.

Zack, T., Brumm, R., 1998. Ilmenite/liquid partition coefficients of 26 trace elements determined through ilmenite/clinopyroxene partitioning in garnet pyroxenite. In: Gurney, J.J., Gurney, J.L., Pascoe, M.D., Richardson, S.H. (Eds.), 7th International Kimberlite Conference. In: Red Roof Design, Cape Town, 986–988.

Ziberna, L, Nimis, P, Zanetti, A., Marzoli, A., Sobolev N.V., 2013. Metasomatic Processes in the Central Siberian Cratonic Mantle: Evidence from Garnet Xenocrysts from the Zagadochnaya Kimberlite. Journal of Petrology 54, 2379–2409.

983

984 **Figure captions**

985 Fig. 1. Location of Dalnyaya pipe within the YKP and Daldyn-Alakit kimberlite fields in
986 Siberian platform. (A) General scheme of Siberian craton and kimberlite fields. (B) Scheme of
987 the area around Dalnyaya pipe from Google maps.

988

989 Fig. 2. Scanned images of thin sections of mantle xenoliths from Dalnyaya pipe. (A-C) Ilmenite
990 megacrysts with clinopyroxene and polyphase inclusions; (D) low-Cr websterite. E, F:
991 clinopyroxene-rich clusters in garnet lherzolites; (F, G, J) garnet-rich clusters in peridotite; (H, P)
992 orthopyroxene-rich clusters in garnet lherzolites; (L, R) deformed peridotites; (K, N, S)
993 porphyroclastic peridotites; (M, O, W) ilmenite-bearing vein in garnet peridotite; (T)
994 fragmentation of peridotite – and clinopyroxenite by protokimberlite melt; (U) garnet peridotite
995 interacted with melt; (V) garnet harzburgite; (X) coarse garnet dunite

996

997 Fig. 3. Compositions of the pyropes (A) from AKB, (B) PK and (C) peridotitic xenoliths from
998 Dalnyaya pipe. In Cr_2O_3 vs CaO plot, the composition of garnets from Rodionov et al. (1984) are
999 shown by small dots. In addition the analyses of the mineral grains from xenoliths and those
1000 analyzed by ICP are shown by stars (see legend).

1001

1002 Fig.4. Compositions of Cr-diopsides from (A) AKB; (B) PK and (C) peridotitic xenoliths from
1003 Dalnyaya pipe.

1004

1005 Fig. 5. Compositions of chromites in peridotitic xenoliths from Dalnyaya pipe and from (A)AKB
1006 and (B)PK according to Rodionov et al.(1984).

1007

1008 Fig.6. Compositions of ilmenites from AKB (A) and PK (B) from Dalnyaya pipe. In addition the
1009 analyses of the mineral grains from xenoliths and those analyzed by ICP are shown by stars (see
1010 legend).

1011

1012 Fig.7. Compositions of phlogopites from mantle xenoliths from Dalnyaya pipe. Fields of
1013 disseminated and veined phlogopites from Sytykanskaya (Ashchepkov et al., 2015) pipe are also
1014 plotted

1015

1016 Fig.8. Variation diagrams for olivines from mantle xenoliths from Dalnyaya pipe relative to $Fe^{\#}$
1017 from the routine EPMA analyses.

Fig.9. Comparison of the Orthopyroxene-based geotherm. (A) Opx *T* (^{o}C) (Brey and Kohler, 1990) –*P* (GPa) (McGregor, 1974) and *P*–*T* estimates obtained with other combinations of thermobarometers; (B) *P* (GPa) (Brey and Kohler, 1990) –*T* (^{o}C) by Cpx; (C) *P* (GPa) (Brey and Kohler, 1990) and *T* (^{o}C) by Opx. *T* (^{o}C) (Brey and Kohler, 1990) and *P* (GPa) by (Nickel and Green, 1985); (D) *P*–*T* by (Nimis and Taylor, 2000); (E) *T* (^{o}C) (Nimis and Taylor, 2000Cor)–*P* (GPa) (Ashchepkov et al., 2015Cpx); (F) T (^{o}C) (O'Neil and Wood,1979 Mono) – P (GPa) (Ashchepkov et al., 2015Gar).

Fig. 10. (A) *P*–*T*–*X*–*f*(O_2) diagram for minerals from xenoliths found in Dalnyaya pipe kimberlite. 140 xenoliths from our collection and some associations from Rodionov and colleagues (1983, 1993); (B) *P*–*T*–*X*–*f*(O_2) diagram for the minerals from the heavy mineral separates of PK; (C) *P*–*T*–*X*–*f*(O_2) diagram for the minerals from the heavy mineral separates of ABK. Symbols: 1. Opx: *T* (^{o}C) (Brey and Kohler, 1990) vs *P* (GPa) (McGregor, 1974). 2. Cpx: *T* (^{o}C) vs *P* (GPa) (Nimis and Taylor, 2000); 3. *T* (^{o}C) (Nimis and Taylor, 2000) vs *P* (GPa) (Ashchepkov et al., 2011); 4. same for pyroxenites; 5. The same for pyroxenes analyzed by ICP. for garnets: 6. *T* (^{o}C) (O'Neill and Wood, 1979)–*P* (GPa) (Ashchepkov et al., 2010), Chromite 7. *T* (^{o}C) (O'Neill and Webb, 1987)–*P* (GPa) (Ashchepkov et al., 2010); 8. Ilmenite megacrysts *T* (^{o}C) (Taylor et al., 1998) – (Ashchepkov et al., 2010); 9. The same for xenoliths; 10. For Olivines $Fe^{\#}$–*P* (GPa) (Ashchepkov et al., 2011) (Cpx associated with Ol); 11. *T* (^{o}C)–*P* (GPa) (Brey and Kohler, 1990). In the *P*–*T* plot the approximate the diamond-graphite transition Kennedy and Kennedy (1976) is shown. In *P*–*f*(O_2) plot the diamond stability field is after Stagno and Frost (2013).

Fig. 11. REE and spider diagrams for minerals from peridotitic xenoliths from the Dalnyaya pipe. Normalization to primitive mantle (PM) after McDonough and Sun (1995).

Fig. 12. REE and spider diagrams for ilmenite megacrysts and their clinopyroxene Inclusions(A) and the minerals from concentrates of the Dalnyaya pipe(B). Normalization to primitive mantle after McDonough and Sun (1995).

Fig. 13. REE and spider diagrams for calculated melts in equilibrium with (A) clinopyroxenes, K_D after (Hart and Dunn, 1993); (B) olivines and orthopyroxene, K_D after (Ionov et al., 1995); (C) garnets from refertilized peridotites, (D) ilmenite megacrysts and their clinopyroxene

inclusions. The dashed lines represent the range of kimberlite compositions in Dalnyaya pipe after Kargin et al. (2011). Partition coefficients for clinopyroxenes (Hart and Dunn, 1993), for garnets (Green et al., 2000) and for ilmenites (Zack and Brumm, 1998; Klemme et al., 2006). Normalization to primitive mantle after McDonough and Sun (1995).

Fig. 14. Partition coefficients determined. (A) Clinopyroxenes /garnet for the relatively equilibrated associations garnet-clinopyroxenes; (B) clinopyroxenes /ilmenite for the ilmenite-clinopyroxene intergrowths and calculated ilmenite-melt coefficient for the sample DL175. Normalization to primitive mantle after McDonough and Sun (1995).

Fig. 15. Different variations of protokimberlite melt evolution (calculated according to AFC model of DePaolo, 1981) and compositions of the minerals in equilibrium. (A) Gar from melt assimilating Cpx (R=0.5); (B) Cpx from melt assimilating Gar; (C) Cpx from melt assimilating Opx (R=0.5); (D) Gar from melt assimilating Ilm. K_D for Gar/Melt (Green at al., 2000), for Cpx (Hart and Dunn, 1993). Normalization to primitive mantle after McDonough and Sun (1995).

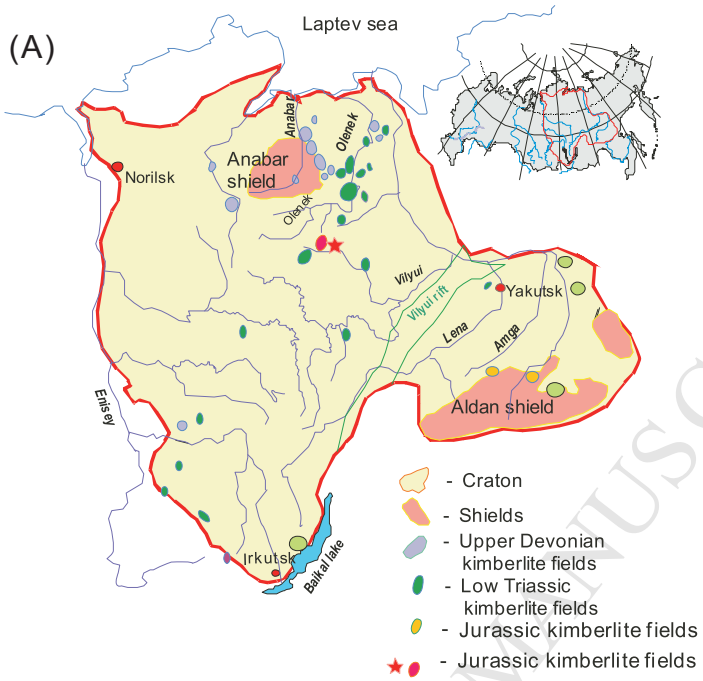
(A)
Laptev sea
Norilsk
Anabar shield
Anabar
Olenek
Olenek
Vilyui
Vilyui rift
Yakutsk
Lena
Anga
Aldan shield
Yenisey
Irkutsk
Baikal lake
- Craton
- Shields
- Upper Devonian kimberlite fields
- Low Triassic kimberlite fields
- Jurassic kimberlite fields
- Jurassic kimberlite fields


(B)
Udachnaya
Zarnitsa
Dolgozhdannaya
Sytykanskaya
Zagadochnaya
Dalnyaya

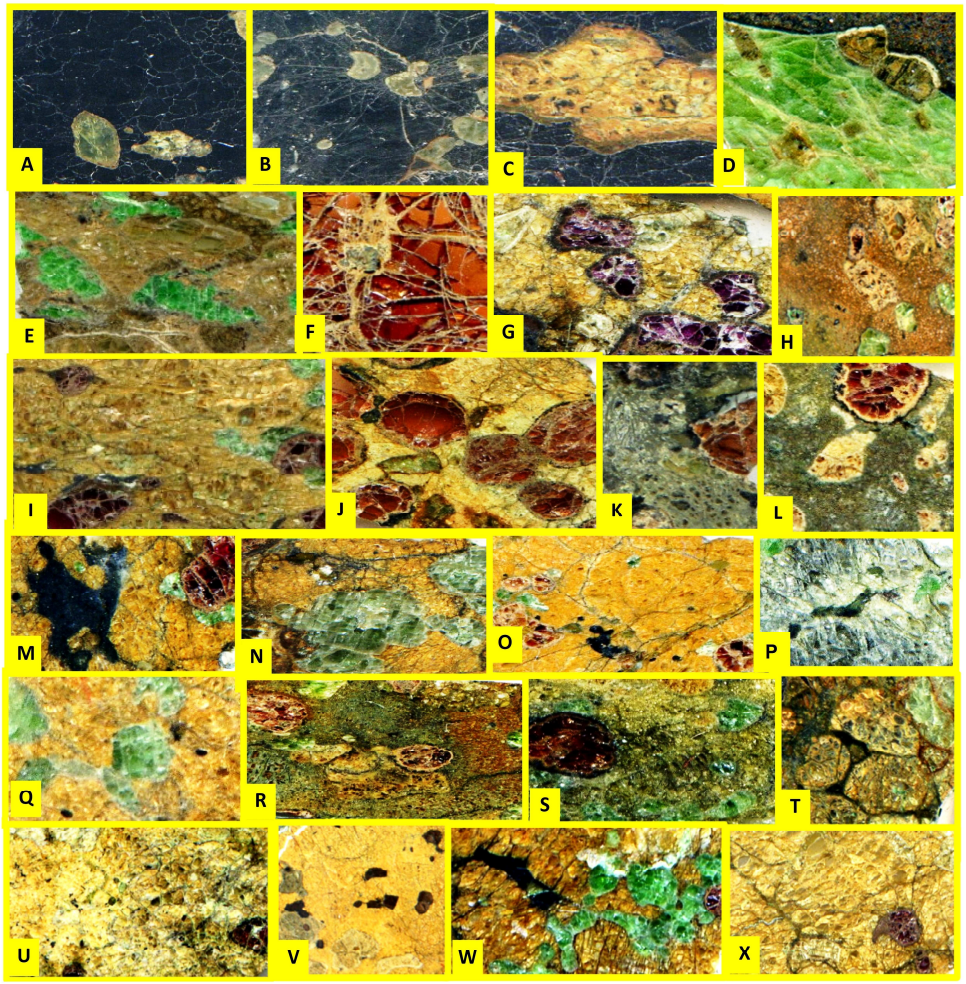

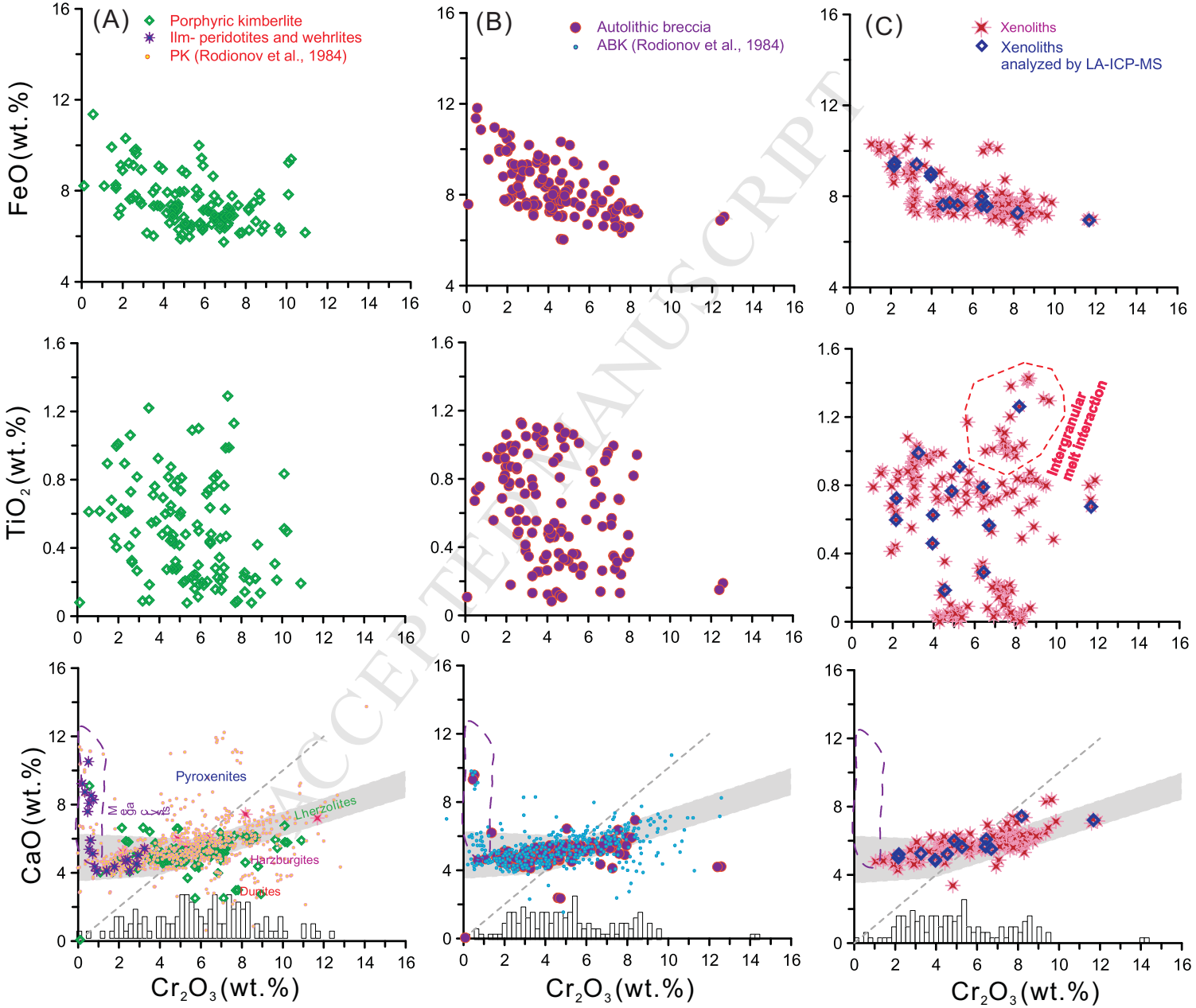

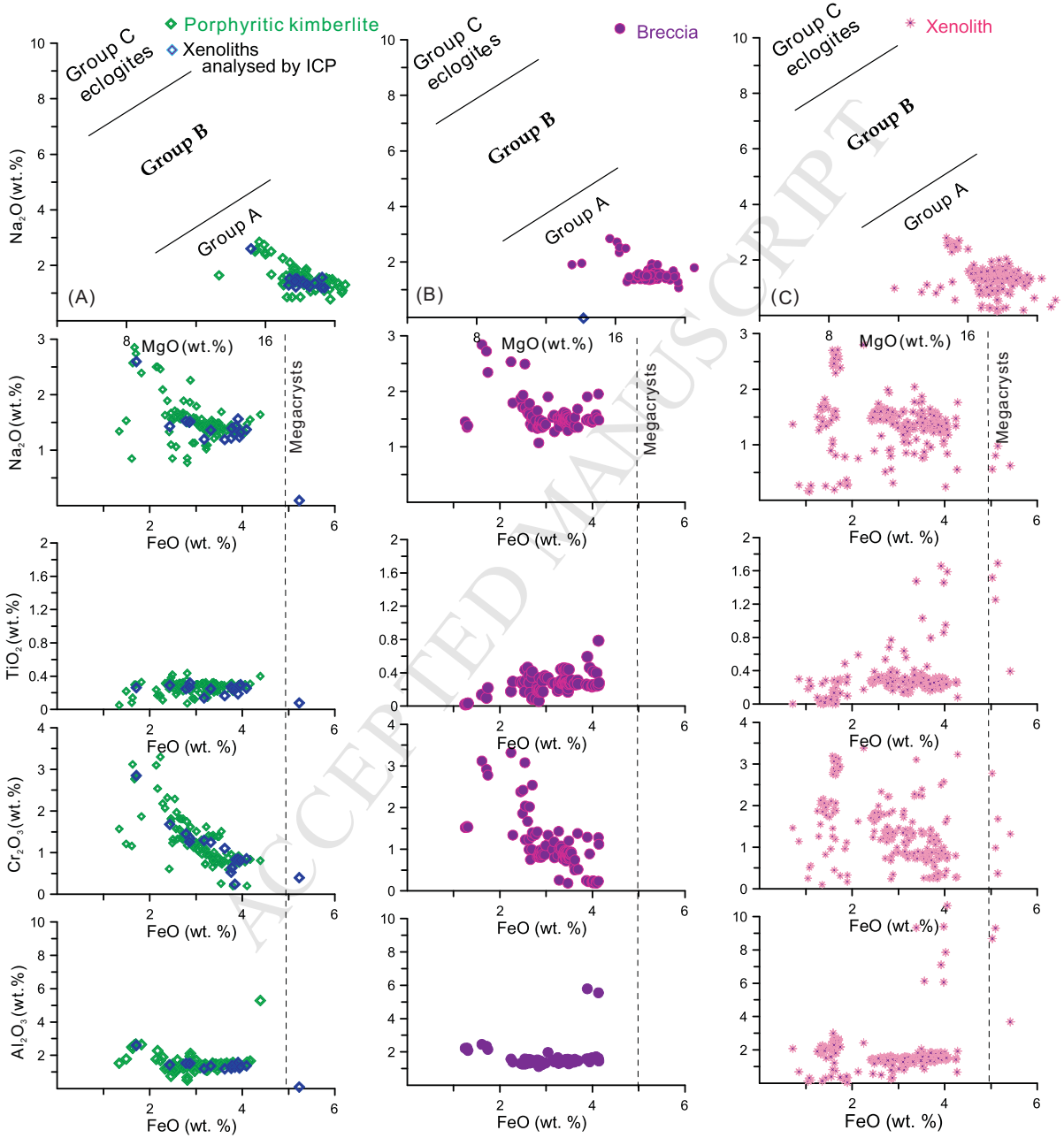

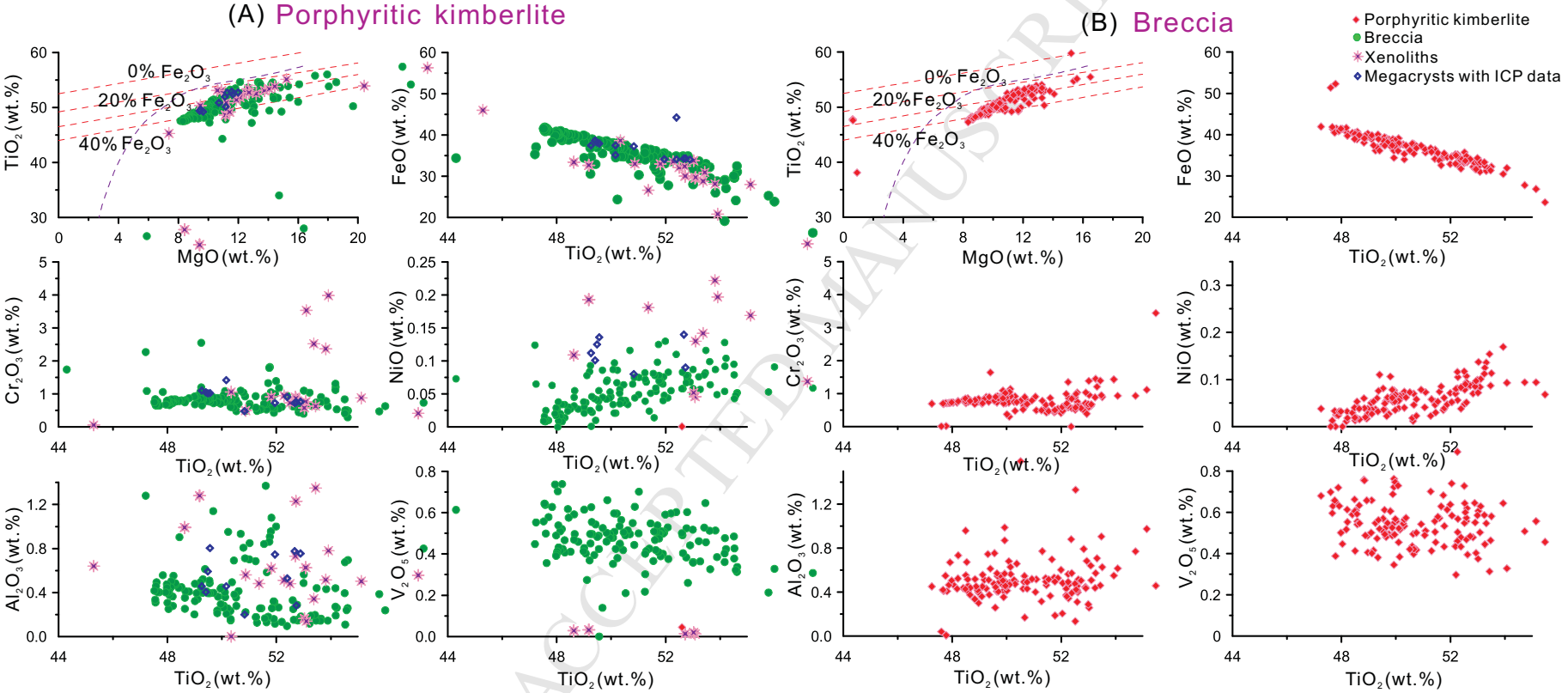

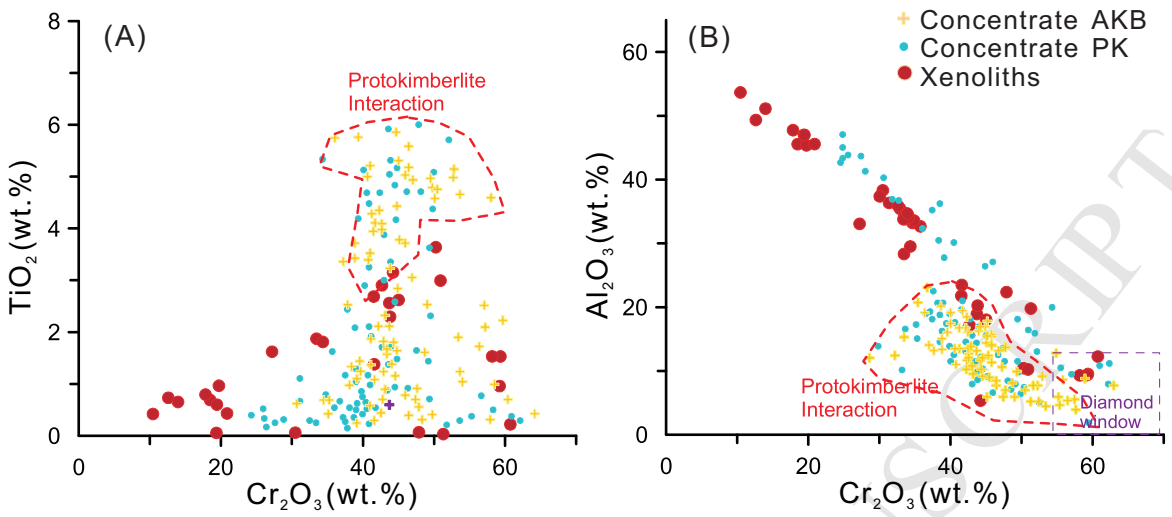

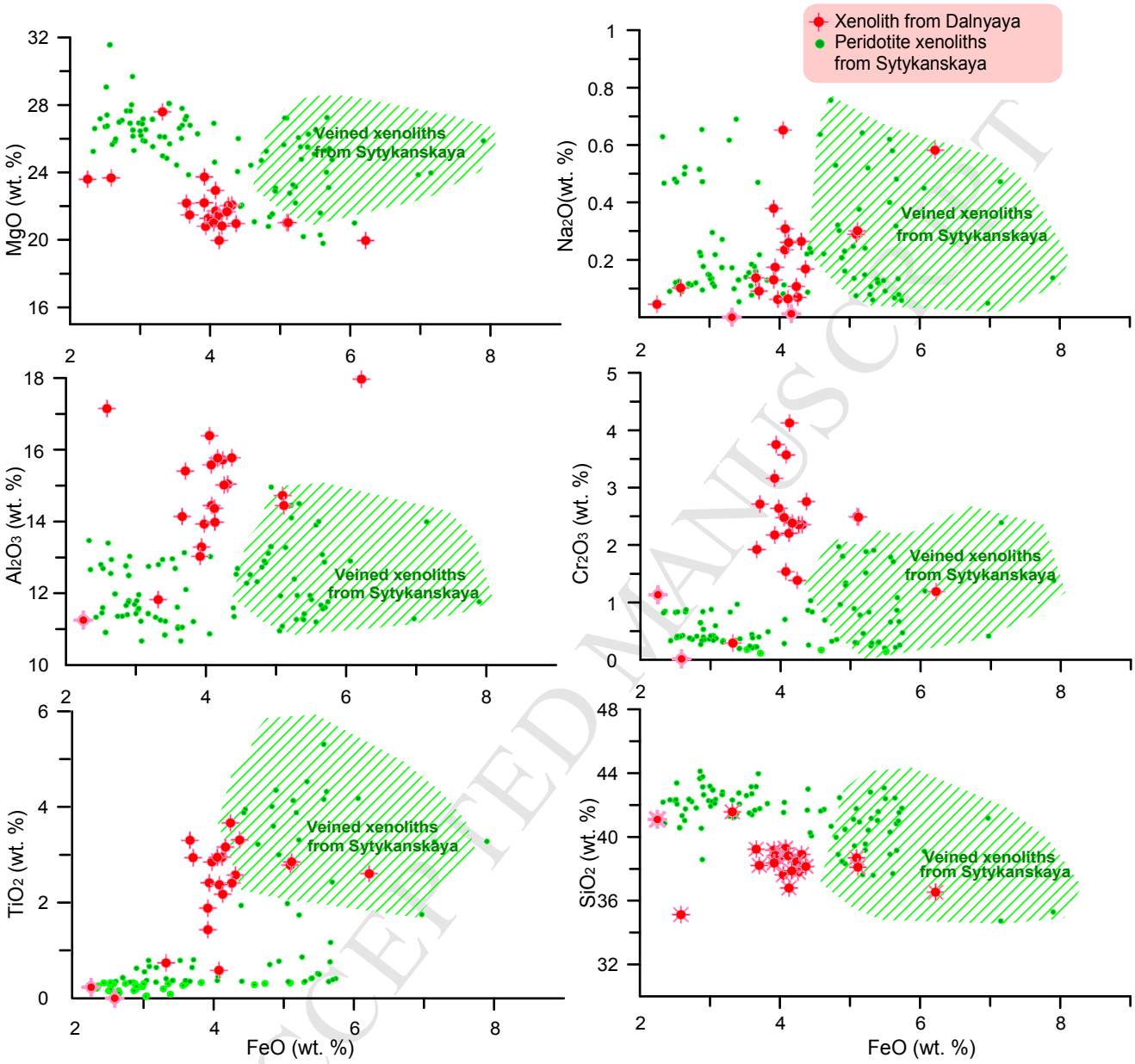

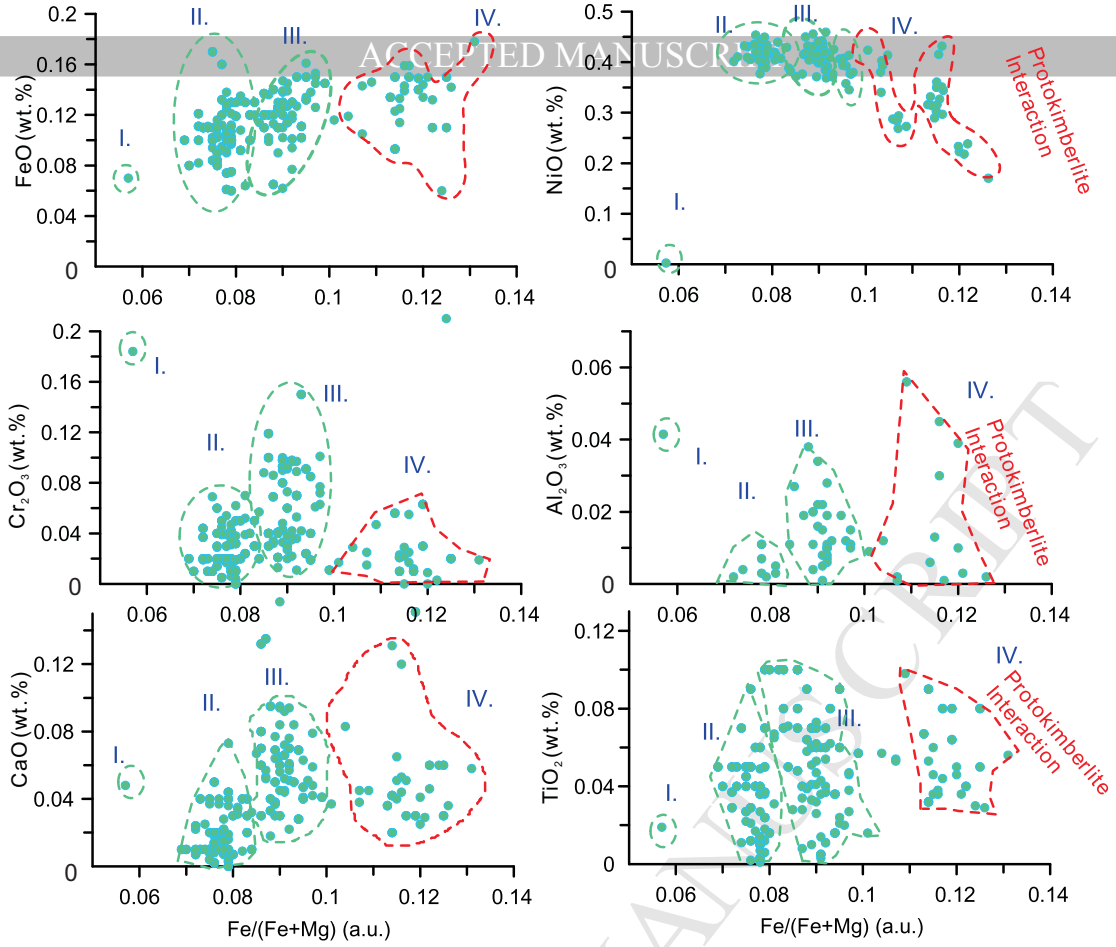

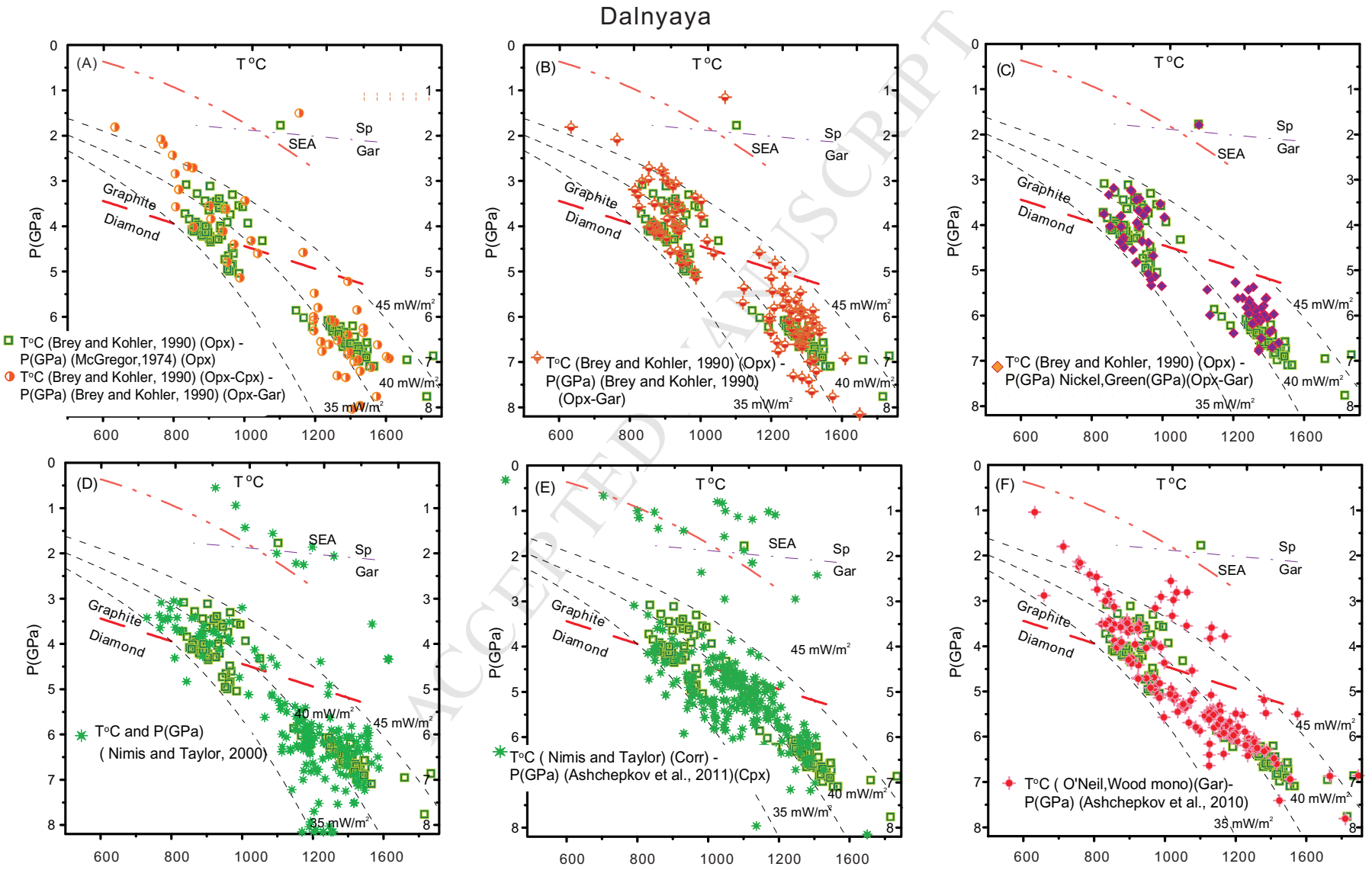

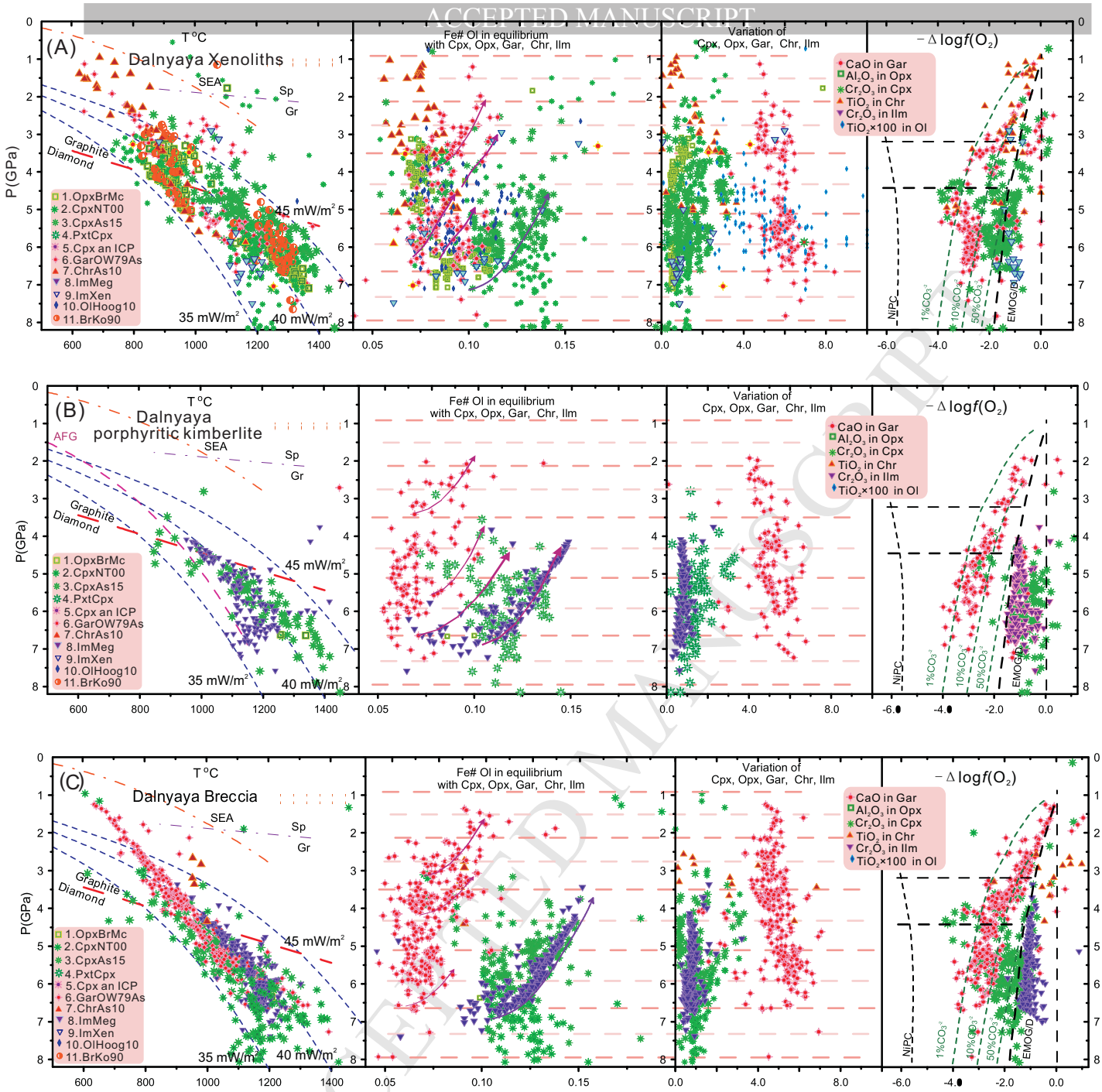

Dalnyaya all peridotitic minerals ananlyzed by LA-ICP-MS in thin sections

Minerals from peridotite xenoliths

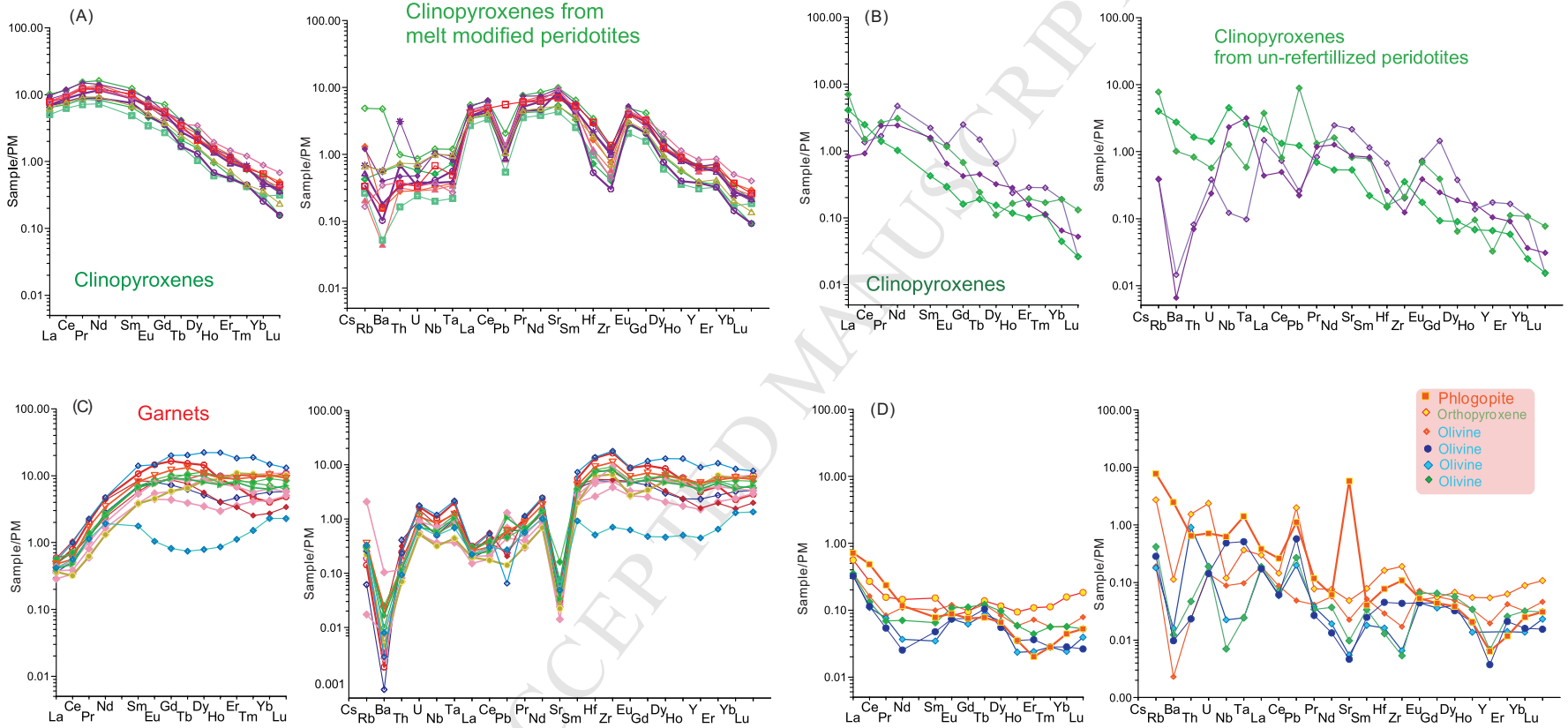

Fig.12

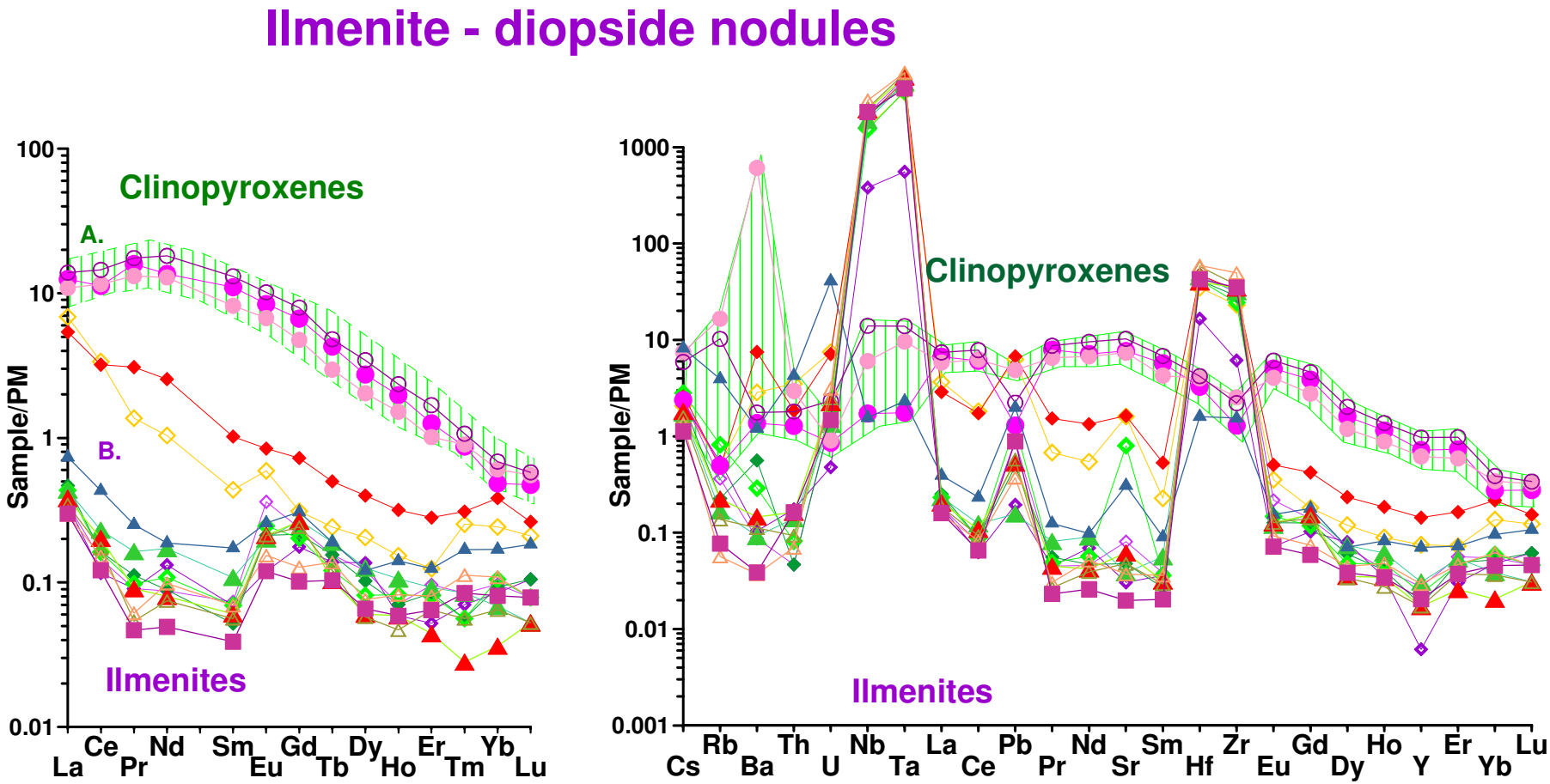
Ilmenite - diopside nodules
Clinopyroxenes
A.
B.
Ilmenites
Sample/PM
100
10
1
0.1
0.01
La Ce Pr Nd Sm Eu Gd Tb Dy Ho Er Tm Yb Lu
Clinopyroxenes
Ilmenites
1000
100
10
1
0.1
0.01
0.001
Cs Rb Ba Th U Nb Ta La Ce Pb Pr Nd Sr Sm Hf Zr Eu Gd Dy Ho Y Er Yb Lu

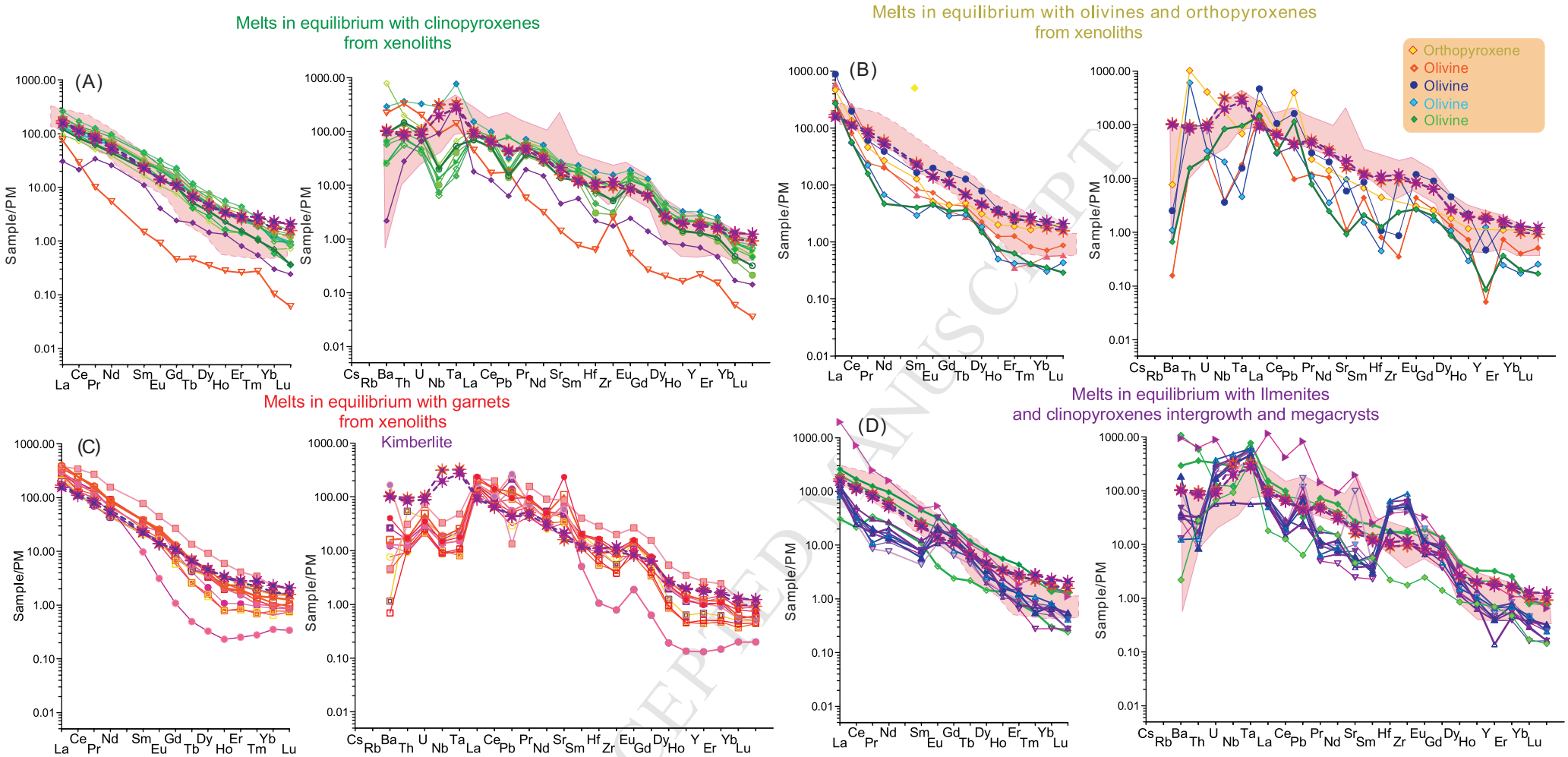

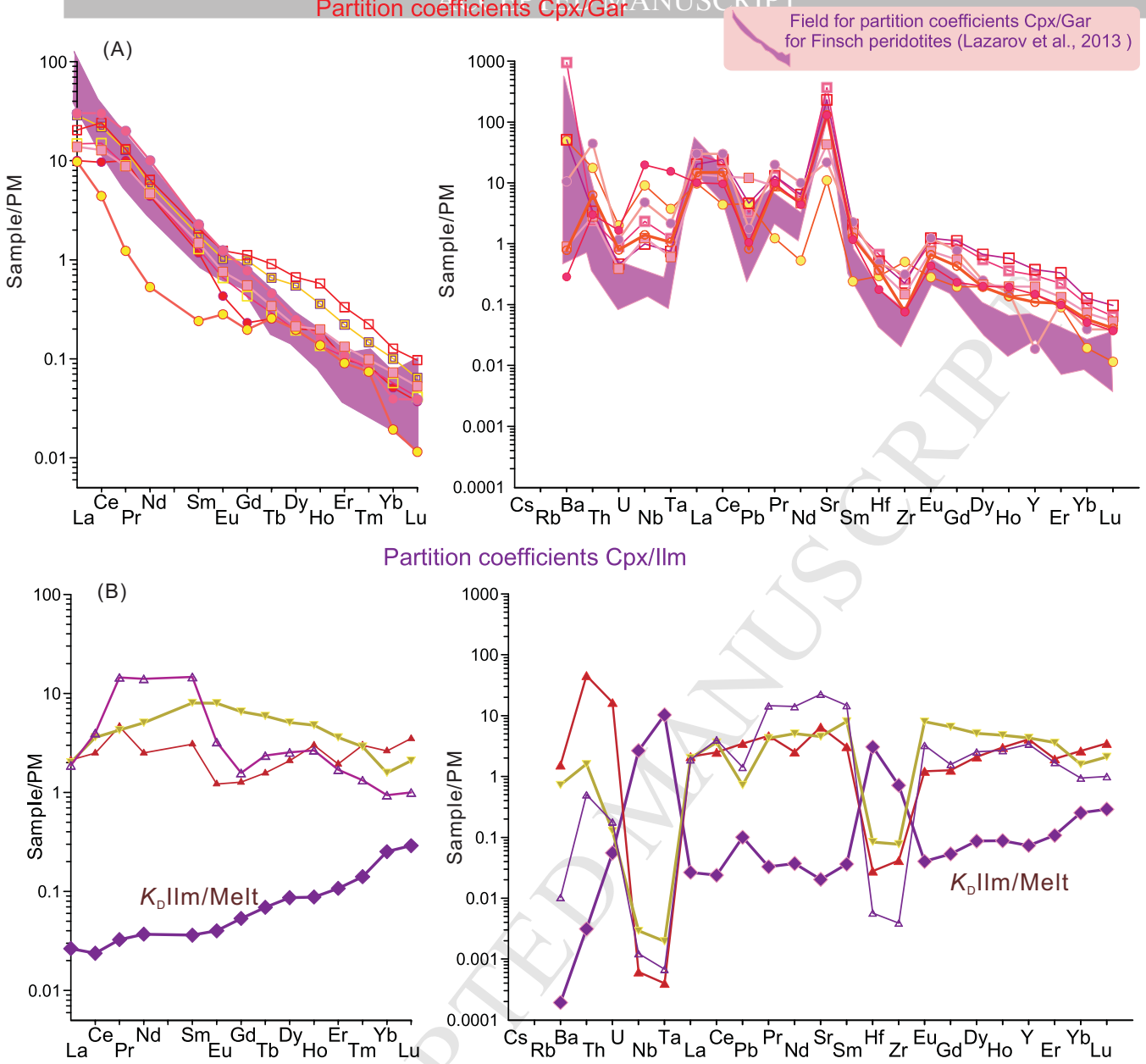

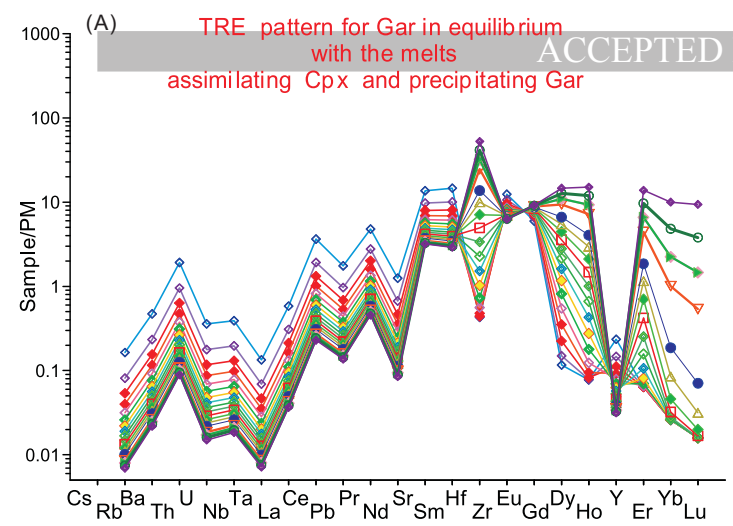

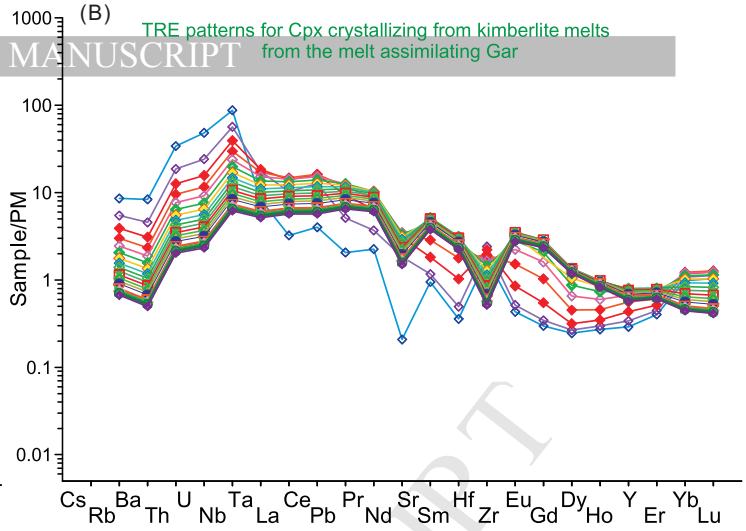

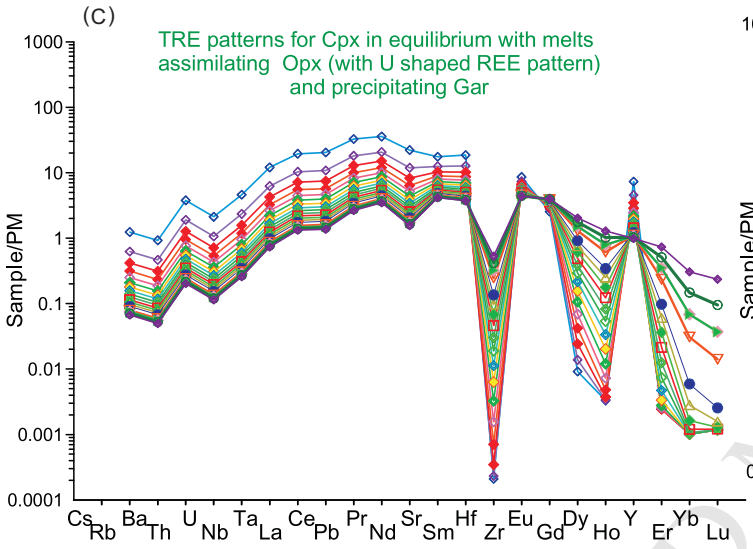

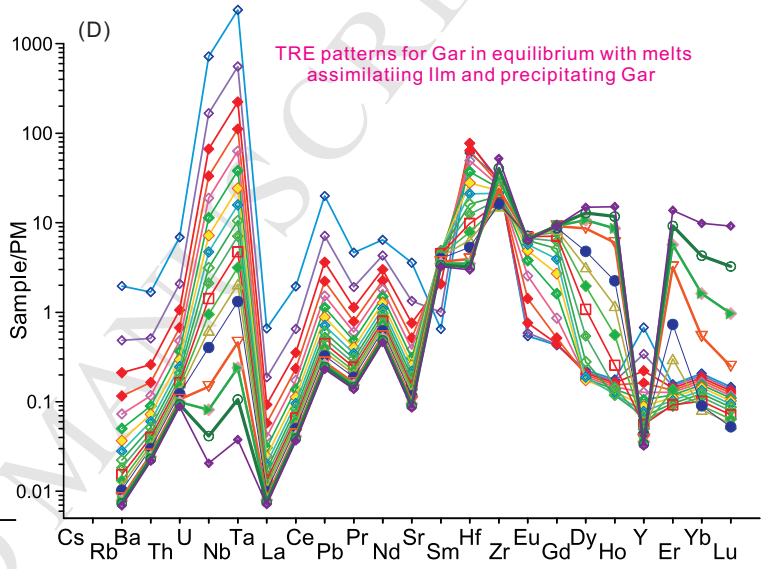

- Mantle column beneath Dalnyaya kimberlite pipe consist of several (5) layers heated from bottom
- Peridotite mantle beneath Dalnyaya interacted with protokimberlite melts in several stages
- Many mineral associations in the mantle column are not thermally and chemically equilibrated
- SCLM beneath Dalnyaya pipe contains only small amounts of eclogites and pyroxenites